

# A parallel Dynamic Mode Decomposition algorithm using modified Full Orthogonalization Arnoldi for large sequential snapshots

Sreevatsa **Anantharamu**<sup>a</sup>, Krishnan **Mahesh**<sup>a,\*</sup>

<sup>a</sup>*Department of Aerospace Engineering and Mechanics, University of Minnesota, Minneapolis, Minnesota 55414, USA*

## ARTICLE INFO

### Article history:

Received 1 May 2013

Received in final form 10 May 2013

Accepted 13 May 2013

Available online 15 May 2013

Communicated by S. Sarkar

## ABSTRACT

A novel technique based on the Full Orthogonalization Arnoldi (FOA) is proposed to perform Dynamic Mode Decomposition (DMD) for a sequence of snapshots. Two modifications to Full Orthogonalization Arnoldi are discussed for situations where the matrix  $A$  whose FOA is to be performed is unknown, but the vectors  $A^{t-1}v_1$  are known. Finite precision error analysis is performed on both variants, and the one with better numerical properties is used as a kernel in the proposed Full Orthogonalization Arnoldi Dynamic Mode Decomposition (FOADMD) algorithm. The proposed method i) does not require Singular Value Decomposition (SVD) if the snapshot matrix has a reasonable condition number, ii) results in projected matrices whose eigenvalues and eigenvectors can be reliably computed in floating point arithmetic, iii) lends itself to easy parallelism as the main computational kernel involves only vector additions and dot products and iv) requires only one snapshot at a time, rather than all snapshots at once. Hence, the new technique is well-suited for DMD of large datasets on parallel computing platforms. It is shown that for FOADMD and SVD-based DMD method without rank truncation, the finite precision error in the computed projection of  $A$  is  $O(\epsilon_m \kappa_2(X))$ , where  $X$  is the matrix of snapshots,  $\kappa_2(X)$  is the 2-norm condition number of the snapshot matrix and  $\epsilon_m$  is the relative round-off error or machine epsilon. Based on finite precision error analysis, rank truncated FOADMD is proposed to accurately compute the projected linear mapping  $A$  when the condition number of snapshot matrix is  $O(1/\epsilon_m)$ . Error indicators that indicate the quality of the obtained DMD eigenvector and DMD eigenvalues to devise stopping criterions for DMD are also presented and validated. The DMD eigenvalues and eigenvectors obtained from the implementation of FOADMD are compared to SVD-based DMD methods for a variety of problems of increasing dimensionality and varying condition number of snapshot matrix.

© 2019 Elsevier Inc. All rights reserved.

\*Corresponding author: Tel.: +1-612-624-4175; fax: +0-000-000-0000;  
e-mail: [kmahesh@umn.edu](mailto:kmahesh@umn.edu) (Krishnan Mahesh)

## 1. Introduction

Numerical simulations of both laminar and turbulent flows with  $O(10^{5-10})$  degrees of freedom generate high dimensional datasets comprising of velocity and pressure field at multiple time instants. These datasets can be low dimensional when expressed in appropriate bases, often interchangeably termed as ‘modes’. The high dimensional dataset can be represented as a linear combination of few of these modes to reasonable accuracy. A review of different modal decomposition techniques to identify these modes for fluid flows is given in Taira et al. (2017) and Rowley and Dawson (2017).

Dynamic Mode Decomposition (DMD) is a data-driven modal decomposition technique that identifies a set of modes from multiple snapshots of the observable vectors (defined later in section 2.1). Each of these modes are assigned an eigenvalue which denotes growth/decay rate and oscillation frequency of the mode. The obtained modes and corresponding eigenvalues together capture the dynamics of the underlying system. Rowley et al. (2009) related the DMD modes and DMD eigenvalues to the eigenfunctions and eigenvalues of the Koopman operator. The Koopman operator (Mezić, 2013) is an infinite dimensional linear operator that describes the evolution of linear and nonlinear dynamical systems. These connections make DMD applicable to nonlinear systems such as those governed by the Navier–Stokes equations.

DMD for sequential snapshots uniformly separated in time was first introduced by Schmid and Sesterhenn (2008). Schmid (2010) proposed two algorithms to perform DMD. One was based on Arnoldi with no orthogonalization, and the other relied on singular value decomposition (SVD) of the sequence of snapshots. The SVD based method was seen to have better finite precision accuracy than the Arnoldi based method. Tu et al. (2013) proposed DMD for snapshot pairs instead of sequence of snapshots. They also proposed Exact DMD where the DMD modes and eigenvalues are defined as the eigendecomposition of the minimum Frobenius norm mapping that relates the snapshot pairs in a least-squares sense. Hemati et al. (2014) formulated a low storage version of the algorithm proposed by Tu et al. (2013) to process large and streaming datasets and a compression procedure to reduce the effect of noise in the dataset on the DMD modes and eigenvalues. Williams et al. (2015) proposed Extended DMD where they compute approximate Koopman eigenfunctions and Koopman eigenvalues from DMD. Williams et al. (2014) proposed Kernel DMD where a large set of observables were incorporated into the DMD algorithm at nearly the same cost that one would have choosing observables as the system states. This was possible by reformulating Extended DMD such that only the inner product of observables needs to be computed. These inner products were efficiently computed through kernels on the system states. Jovanović et al. (2014) proposed sparsity-promoting DMD to choose dynamically important DMD modes. The coefficients of the first snapshot in the basis of DMD modes is not always an indicator of the contribution of the DMD mode to the entire dataset. A DMD mode with large coefficient can also have a large decay rate (given by the corresponding DMD eigenvalue). They proposed a methodology to rank DMD modes by the extent to which they explain the entire dataset. Modes with eigenvalues close to the unit circle are chosen and those with large coefficients but higher decay rates are avoided. A parallel version of the DMD algorithm proposed in Schmid (2010) was presented in Sayadi and Schmid (2016). The underlying parallel algorithm used the TSQR algorithm

of Demmel et al. (2012) followed by SVD of a small upper triangular matrix. Numerical experiments on the error due to the number of snapshots and spatial resolution for synthetically generated data with noise were carried out in Duke et al. (2012), and that due to the choice of observables is presented in Zhang et al. (2017).

In this paper, since we propose a Arnoldi-based method, we work with a sequence of snapshots. The objective of this paper is to i) present a modification to the Arnoldi method with full orthogonalization such that it can be used to perform DMD, ii) perform finite precision arithmetic error analysis of the method and iii) present indicators for the quality of the obtained DMD modes and eigenvalues. The paper is organized as follows. In section 2, we first present a brief description of DMD and discuss some of the previous methods in the well known Galerkin framework. Arnoldi based DMD variant-1 is then presented which uses modified Arnoldi variant-1 to obtain the projected upper Hessenberg matrix and the Arnoldi vectors. Finite precision error analysis of modified Arnoldi variant-1 leads us to modified FOA method which is the kernel of the proposed FOADMD algorithm discussed at the end of section 2. In section 3, we discuss properties of the FOADMD method such as error analysis of floating point arithmetic implementation, error indicators for obtained eigenvector and eigenvalue pair, exact reconstruction property, operation count, parallel implementation scaling and streaming aspects of the method. In section 4, we finally demonstrate FOADMD algorithm on four test cases: i) synthetically generated dataset, ii) flow over a circular cylinder at  $Re = 100$ , iii) linearized channel flow and iv) jets in cross-flow at two different jet velocity to cross flow velocity ratios.

## 2. Dynamic Mode Decomposition algorithm

### 2.1. Some previous DMD methods

We first discuss a framework (Rowley and Dawson, 2017) to present DMD methods. Then, Arnoldi method with no orthogonalization (Schmid, 2010; Rowley et al., 2009; Williams et al., 2015) and SVD based approach (Schmid, 2010) is presented. Note that we will be dealing with what are called projected DMD methods (Tu et al., 2013).

Let  $x_j \in \mathbb{C}^n$  be the state of system at time  $t_j$ . The states  $x_j$  are assumed to be equally spaced in time. i.e.  $t_j = (j - 1)\Delta t$  where  $\Delta t$  is the time separation between successive states. Let  $\psi(x) := [\psi^1(x) \quad \psi^2(x) \quad \dots \quad \psi^M(x)]^T$  be a vector of functions i.e. each  $\psi^i(x) : \mathbb{C}^n \rightarrow \mathbb{C}$ . Each  $\psi^i(x)$  is called an observable (Rowley et al., 2009).  $\psi(x)$  is also called as vector of observables. Snapshot vector  $\psi_j \in \mathbb{C}^M := \psi(x_j)$ . i.e.  $\psi_j = [\psi^1(x_j) \quad \psi^2(x_j) \quad \dots \quad \psi^M(x_j)]^T$ . Let  $X_i^j \in \mathbb{C}^{M \times (j-i+1)}$  be the snapshot matrix formed by stacking the snapshot vectors from time  $t_i$  to  $t_j$  separated by constant time intervals as columns.

$$X_i^j := [\psi_i \quad \psi_{i+1} \quad \dots \quad \psi_{j-1} \quad \psi_j] \quad (1)$$

A common state vector is the velocity at all points in the domain of fluid simulation and a common vector of observables is the state vector itself.

Let  $N$  be the total number of snapshots. A linear mapping  $A$  is assumed to relate the successive snapshot vector as

$$\psi_{i+1} = A\psi_i, \quad (2)$$

$$X_2^N = AX_1^{N-1}. \quad (3)$$

Our interpretation of linear mapping  $A$  is discussed in section 2.2.1. Let  $\chi_i^j$  be the subspace of  $\mathbb{C}^M$  associated with the range of snapshot matrix  $X_i^j$ . Note that the columns of  $X_1^N$  need not be basis vectors for the subspace  $\chi_1^N$  as they can be linearly dependent. Following the assumption of the linear mapping,  $\chi_1^N$  then becomes a Krylov subspace,

$$K_N(A, \psi_1) := \text{span}\{\psi_1, A\psi_1, \dots, A^{N-1}\psi_1\}. \quad (4)$$

If the snapshots are linearly dependent, then  $N$  is modified to include the linearly independent snapshot sequence only. So,  $\chi_1^N$  and  $K_N(A, \psi_1)$  represent the same subspace.

If sufficient number of snapshots of a numerical simulation or experimental visualization are collected, then  $X_1^N$  has information of the physical processes associated with fluid flow. After collecting large number of snapshots, one might expect that adding an additional snapshot will not appreciably modify the subspace  $\chi_1^N$ . Then, it should be possible to approximate the last snapshot  $\psi_N$  as a linear combination of the previous  $N - 1$  snapshots.

$$\psi_N = \sum_{i=1}^{N-1} c_i \psi_i + r \quad (5)$$

where  $r$  is the residual vector. One could obtain the best possible coefficient  $c_i$ 's by minimizing  $\|r\|_2$  (If  $x \in \mathbb{C}^M$ , then  $l^2$  norm of  $x$  is defined as  $\|x\|_2 := \left(\sum_{i=1}^M |x_i|^2\right)^{1/2}$ ). Let  $c$  be the coefficient vector  $[c_1 \dots c_{N-1}]^T$ . Then, the following least square problem can be defined to obtain  $c$  whose solution is given by the normal equations,

$$c = \arg \min_{d \in \mathbb{C}^{N-1}} \|\psi_N - X_1^{N-1} d\|_2. \quad (6)$$

The solution to the above problem is

$$c = \left( X_1^{N-1H} X_1^{N-1} \right)^{-1} \left( X_1^{N-1H} \psi_N \right), \quad (7)$$

where  $X_1^{N-1H} \in \mathbb{C}^{N \times M}$  is the adjoint of matrix  $X_1^{N-1} \in \mathbb{C}^{M \times N}$ .

The solution to the above least square problem is equivalent to saying that the  $r$  vector is orthogonal to the subspace  $\chi_1^{N-1}$ . When the condition of number of snapshot matrices is large, the computed  $c$  will have large finite precision error. Techniques based on QR decomposition and SVD to solve equation 6 do not have this drawback (Trefethen and Bau III, 1997). We can combine equations 3 and 5 to obtain

$$X_2^N = A X_1^{N-1} = X_1^{N-1} C + r e_{N-1}^H, \quad (8)$$

where,

$$C = \begin{bmatrix} 0 & 0 & \dots & \dots & 0 & c_1 \\ 1 & 0 & \ddots & \dots & 0 & c_2 \\ 0 & 1 & \ddots & \ddots & \vdots & \vdots \\ \vdots & \vdots & \ddots & \ddots & \ddots & \vdots \\ \vdots & \vdots & \ddots & 1 & 0 & c_{N-2} \\ \vdots & \vdots & \ddots & \ddots & 1 & c_{N-1} \end{bmatrix} \quad (9)$$

is a upper Hessenberg matrix. This technique is a special case of the standard Arnoldi method with partial orthogonalization with the previous Arnoldi vectors (Saad, 1980). Next, consider the well-known Galerkin projection to

obtain approximate eigenvectors (also called “Ritz vectors”) and approximate eigenvalues (also called “Ritz values”) of  $A$  from the subspace  $\chi_1^{N-1}$ . The eigenvalues and eigenvectors of  $C$  can be used to obtain approximate eigenvalues and eigenvectors of the linear mapping  $A$ . The Galerkin statement is : Find  $\lambda \in \mathbb{C}, v \in \chi_1^{N-1}$  pair s.t.  $Av - \lambda v \perp \chi_1^{N-1}$ . Suppose  $X_1^{N-1}$  forms a basis for  $\chi_1^{N-1}$ , we then have  $v = X_1^{N-1}z$  and

$$\begin{aligned} X_1^{N-1H} [AX_1^{N-1}z - \lambda X_1^{N-1}z] &= 0, \\ X_1^{N-1H} AX_1^{N-1}z &= \lambda X_1^{N-1H} X_1^{N-1}z. \end{aligned} \quad (10)$$

Using equation 8 and the fact that  $r$  is orthogonal to  $\chi_1^{N-1}$ , we obtain

$$X_1^{N-1H} X_1^{N-1} Cz = X_1^{N-1H} X_1^{N-1} \lambda z \quad (11)$$

or

$$Cz = \lambda z \quad (12)$$

which is a small eigenvalue problem of size  $(N - 1) \times (N - 1)$ . Let  $\lambda_i$  and  $z_i$  be the  $i^{th}$  eigenvalue and eigenvector of  $C$ . Then, the eigenvalue  $\lambda_i$  and  $X_1^{N-1}z_i$  are approximate eigenvectors of the linear mapping  $A$ . Since, the subspace used to evaluate the approximate eigenvectors and eigenvalues is that formed by snapshots, the obtained Ritz values and Ritz vectors are also termed as DMD eigenvalues and DMD eigenmodes respectively. Note that equation 10 is equivalent to  $X_1^{N-1H} X_2^N z = \lambda X_1^{N-1H} X_1^{N-1} z$ . To construct  $X_1^{N-1H} X_2^N$  and  $X_1^{N-1H} X_1^{N-1}$ , we only need inner product of observable vectors. Kernel DMD (Williams et al., 2014) uses this trick to efficiently perform DMD with large number of observables.

However, the technique of Arnoldi with no orthogonalization proposed by Schmid (2010) is extremely sensitive to numerical errors. Therefore, a method based on the SVD of the snapshot sequence  $X_1^{N-1}$  was proposed in the same paper. Instead of using  $X_1^{N-1}$  as a basis for  $\chi_1^{N-1}$ , the left singular vectors of  $X_1^{N-1}$  corresponding to the non-zero singular values are used to perform a Galerkin projection. Suppose, the economy SVD of  $X_1^{N-1}$  is given by

$$X_1^{N-1} = U \Sigma W^H, \quad (13)$$

where the columns of  $U$  are the left singular vectors that form an orthogonal basis for range of  $X_1^{N-1}$  or equivalently the subspace  $\chi_1^{N-1}$ ,  $\Sigma$  is the diagonal square matrix with non-zero singular values  $\{\sigma_i\}_{i=1}^{N-1}$  on the diagonal and the columns of  $W$  are the right singular vectors that form an orthogonal basis for the range of  $X_1^{N-1H}$ . Now, using  $U$  as the basis of  $\chi_1^{N-1}$  in the Galerkin projection, we obtain

$$\begin{aligned} U^H [AUz - \lambda Uz] &= 0 \\ U^H AUz &= \lambda z \end{aligned} \quad (14)$$

To evaluate  $U^H AU$ , we use equation 8 and obtain

$$\begin{aligned} AU \Sigma W^H &= X_2^N, \\ AU &= X_2^N W \Sigma^{-1}, \\ U^H AU &= U^H X_2^N W \Sigma^{-1}. \end{aligned} \quad (15)$$

Let  $\tilde{C} := U^H A U$ . Then using equation 15, we can evaluate  $\tilde{C}$  using the snapshot sequence  $X_2^N$  and the SVD of  $X_1^{N-1}$ . The resulting  $\tilde{C}$  matrix will be typically full. The Galerkin statement would then amount to obtaining the eigenvectors and eigenvalues of  $\tilde{C}$ , i.e.

$$\tilde{C}z = \lambda z. \quad (16)$$

If the  $\lambda_i$  and  $z_i$  are the  $i^{th}$  eigenvalue and eigenvector pair for  $\tilde{C}$ , then  $\lambda_i$  and  $Uz_i$  represent the approximate eigenvalue and eigenvector pair of linear mapping  $A$ . In exact arithmetic, both the above methods (SVD-based and Arnoldi-based with no orthogonalization) are equivalent as they pick the same element from the subspace  $\chi_1^{N-1}$ . In finite precision arithmetic, the numerical technique used to solve equation 6 and to obtain SVD determines the finite precision error in Arnoldi-based with no orthogonalization and SVD-based DMD respectively.

The above SVD-based implementation assumes that we use all the singular vectors and singular values resulting from economy SVD of  $X_1^{N-1}$ . Typically, the singular values close to 0 are dropped. The corresponding left and right singular vectors are also dropped. Therefore, in practice, a Galerkin projection on a subspace of  $\chi_1^{N-1}$  is performed. The practical implementation of SVD-based DMD is given in Algorithm 1.

- 1: Form snapshot matrices  $X_1^{N-1}$  and  $X_2^N$
- 2: Perform economy SVD of  $X_1^{N-1}$  i.e.  $X_1^{N-1} = U\Sigma W^H$ . Truncate SVD based on some threshold on the singular values
- 3: Evaluate  $\tilde{C} := U^H X_2^N W \Sigma^{-1}$
- 4: Compute eigenvalues  $\{\lambda_i\}_{i=1}^{N-1}$  and eigenvectors  $\{z_i\}_{i=1}^{N-1}$  of  $\tilde{C}$
- 5: The DMD eigenvalues are  $\{\lambda_i\}_{i=1}^{N-1}$  and DMD eigenvectors are  $\{Uz_i\}_{i=1}^{N-1}$

**Algorithm 1:** SVD-based DMD.

Sayadi and Schmid (2016) proposed a method where instead of SVD of the snapshot matrix  $X_1^{N-1}$ , first a QR decomposition of  $X_1^{N-1}$  is performed. Then, SVD of a small upper triangular matrix  $R$  is performed which leads to the SVD of the entire snapshot matrix  $X_1^{N-1}$ . The QR decomposition of  $X_1^{N-1}$  is carried out using TSQR algorithm of Demmel et al. (2012) which sends lesser number of messages in parallel implementation than a usual QR algorithm.

## 2.2. Arnoldi-based DMD variant-1

The Arnoldi method with full orthogonalization is the most commonly used technique to obtain an orthonormal basis for Krylov subspace. It is mentioned in Schmid (2010) that since the linear mapping  $A$  is not available, Arnoldi method with full orthogonalization cannot be performed in the context of DMD. However, with a modification to the standard Arnoldi method, it is possible to use it to perform DMD. We first describe the classical Arnoldi method and then discuss a modification. Then, Arnoldi-based DMD variant-1 is described and our interpretation of the linear mapping  $A$  is presented and compared to the interpretation by other authors. Then, we perform finite-precision error analysis of the computed quantities with Arnoldi-based DMD variant-1 and motivate the next Arnoldi-based variant, FOADMD.

The classical Arnoldi method to generate an orthonormal basis of Krylov subspace  $K_{N-1}(A, \psi_1)$  is first presented in Algorithm 2.

```

1: Construct initial vector  $v_1$  from the first snapshot.  $v_1 := \frac{\psi_1}{\|\psi_1\|_2}$ 
2: for  $j=1$  to  $N-1$  do
3:    $w = Av_j$ 
4:   for  $i=1$  to  $j$  do
5:      $h_{i,j} = (w, v_i)$ 
6:      $w = w - h_{i,j}v_i$ 
7:   end for
8:    $h_{j+1,j} = \|w\|_2; v_{j+1} = \frac{w}{h_{j+1,j}}$ 
9: end for

```

**Algorithm 2:** Classical Arnoldi method.

The vectors  $v_i$  generated from the above algorithm in addition to being orthonormal satisfy the property (Saad, 2011)

$$\begin{aligned} AV_1^{N-1} &= V_1^N \tilde{H}_N, \\ AV_1^{N-1} &= V_1^{N-1} H_{N-1} + h_{N,N-1} v_N e_{N-1}^H, \end{aligned} \quad (17)$$

where,  $V_1^{N-1}$  represents the matrix formed by stacking vectors  $v_i$ 's ;  $i = 1, \dots, N-1$  as columns. It seems from step 3 of algorithm 2 that we explicitly need to know the mapping  $A$  to perform Arnoldi method. However, the Arnoldi vectors  $v_i$ 's generated by the above algorithm have the following property (Saad, 2011),

$$\text{span}\{v_1, \dots, v_j\} = \text{span}\{\psi_1, \dots, \psi_j\} = \text{span}\{\psi_1, A\psi_1, \dots, A^{j-1}\psi_1\}. \quad (18)$$

Therefore, it should be possible to write

$$v_j = \sum_{k=1}^j \alpha_{k,j} \psi_k. \quad (19)$$

If  $\alpha_{k,j}$ 's are evaluated, then  $Av_j$  can be obtained as

$$Av_j = \sum_{k=1}^j \alpha_{k,j} \psi_{k+1}. \quad (20)$$

Equation 19 can be expressed in matrix form as

$$\begin{bmatrix} v_1 & \dots & v_N \\ \vdots & \vdots & \vdots \end{bmatrix} = \begin{bmatrix} \psi_1 & \dots & \psi_N \\ \vdots & \vdots & \vdots \end{bmatrix} \begin{bmatrix} \alpha_{1,1} & \dots & \alpha_{N,1} \\ 0 & \ddots & \vdots \\ 0 & 0 & \alpha_{N,N} \end{bmatrix}. \quad (21)$$

The matrix of  $\alpha_{i,j}$ 's will be called the  $\alpha$ -matrix which is an upper triangular matrix.

A recursive relation can be derived to compute the column  $\alpha_{1:j+1,j+1}$  using the previously computed portion of  $\alpha$ -matrix i.e.  $\alpha_{1:j,1:j}$  and computed portion of  $H_{N-1}$  matrix i.e.  $H_{1:j+1,1:j}$ .  $v_{j+1}$  generated at the  $j^{th}$  step of Arnoldi method satisfies the relation

$$v_{j+1} = \frac{1}{h_{j+1,j}} \left[ Av_j - \sum_{i=1}^j h_{i,j} v_i \right]. \quad (22)$$

Now, we want to express  $v_{j+1}$  as a linear combination of  $\{\psi_1, \dots, \psi_{j+1}\}$ . Also, the previous  $v_j$ 's have already been expressed as a linear combination of  $\{\psi_1, \dots, \psi_j\}$ . Using this in equation 22,

$$v_{j+1} = \frac{1}{h_{j+1,j}} \left[ A \sum_{k=1}^j \alpha_{k,j} \psi_k - \sum_{i=1}^j h_{i,j} \sum_{k=1}^i \alpha_{k,i} \psi_k \right]. \quad (23)$$

Using the relation that  $\psi_{k+1} = A\psi_k$ , it can be shown that equation 23 is equivalent to

$$v_{j+1} = \frac{1}{h_{j+1,j}} \left[ \sum_{k=1}^j \alpha_{k,j} \psi_{k+1} - \sum_{k=1}^j \sum_{i=k}^j h_{i,j} \alpha_{k,i} \psi_k \right]. \quad (24)$$

The desired form of  $v_{j+1}$  is

$$v_{j+1} = \sum_{k=1}^{j+1} \alpha_{k,j+1} \psi_k. \quad (25)$$

Comparing equation 25 and 24 we obtain

$$\begin{aligned} \alpha_{1,j+1} &= \frac{1}{h_{j+1,j}} \left[ - \sum_{i=1}^j h_{i,j} \alpha_{1,i} \right], \\ \alpha_{k,j+1} &= \frac{1}{h_{j+1,j}} \left[ \alpha_{k-1,j} - \sum_{i=k}^j h_{i,j} \alpha_{k,i} \right]; \quad k = 2, \dots, j, \\ \alpha_{j+1,j+1} &= \frac{1}{h_{j+1,j}} \alpha_{j,j}. \end{aligned} \quad (26)$$

These coefficients can be used in the next step of Arnoldi to evaluate  $Av_j$ . This form the basis of modified Arnoldi variant-1 presented in algorithm 3.

```

1: Construct initial vector  $v_1$  from the first snapshot.  $v_1 := \frac{\psi_1}{\|\psi_1\|_2}$ 
2: for  $j=1$  to  $N-1$  do
3:    $w = \sum_{k=1}^j \alpha_{k,j} x_{k+1}$  //Step replacing  $Av_j$ 
4:   for  $i=1$  to  $j$  do
5:      $h_{i,j} = (w, v_i)$ 
6:      $w = w - h_{i,j} v_i$ 
7:   end for
8:    $h_{j+1,j} = \|w\|_2; v_{j+1} = \frac{w}{h_{j+1,j}}$ 
9:    $\alpha_{1,j+1} = \frac{1}{h_{j+1,j}} \left[ - \sum_{i=1}^j h_{i,j} \alpha_{1,i} \right]$ 
10:  for  $k=2$  to  $j$  do
11:     $\alpha_{k,j+1} = \frac{1}{h_{j+1,j}} \left[ \alpha_{k-1,j} - \sum_{i=k}^j h_{i,j} \alpha_{k,i} \right]$ 
12:  end for
13:   $\alpha_{j+1,j+1} = \frac{1}{h_{j+1,j}} \alpha_{j,j}$ 
14: end for

```

**Algorithm 3:** Modified Arnoldi variant-1.

Equation 17 still holds and the columns of  $V_1^{N-1}$  form a orthonormal basis for the Krylov subspace  $K_{N-1}(A, x_1)$  (same as  $\chi_1^{N-1}$ ). Using  $V_1^{N-1}$  as the basis of  $\chi_1^{N-1}$  in the Galerkin method we obtain

$$H_{N-1} z = \lambda z, \quad (27)$$

where  $H_{N-1}$  is an upper Hessenberg matrix. The DMD eigenmodes are  $V_{N-1} z$  and the DMD eigenvalues are  $\lambda$ . The implementation procedure of the Arnoldi-based DMD variant-1 is given in algorithm 4.

- 1: Form snapshot matrix  $X_1^N$
- 2: Compute  $V_1^{N-1}$  and  $H_{N-1}$  from  $X_1^N$  using modified Arnoldi variant-1 method.
- 3: Compute eigenvalues  $\{\lambda_i\}_{i=1}^{N-1}$  and eigenvectors  $\{z_i\}_{i=1}^{N-1}$  of  $H_{N-1}$
- 4: DMD eigenvalues are  $\{\lambda_i\}_{i=1}^{N-1}$  and DMD eigenvectors are  $\{V_1^{N-1} z_i\}_{i=1}^{N-1}$

**Algorithm 4:** Arnoldi-based DMD variant-1.

### 2.2.1. Interpretation of linear mapping $A$

Suppose vectors  $\psi_i \in \mathbb{C}^M$  denote the observable values at time step  $i$ , then there is a  $R$  such that  $\psi_{R+1} \in \text{span}\{\psi_i\}_{i=1}^R$ . Note that this is will be true for a maximum value of  $R = M$ . So, such a  $R$  always exists. We define  $P$  to be the smallest  $R$  such that  $\psi_{R+1} \in \text{span}\{\psi_i\}_{i=1}^R$ . This means that we can uniquely define a matrix  $\bar{A} \in \mathbb{C}^{P \times P}$  which represents a linear transformation from  $\text{span}\{\psi_i\}_{i=1}^P$  to itself. i.e.  $\text{span}\{\psi_i\}_{i=1}^P$  is the invariant subspace of the defined linear transformation. Suppose columns of  $Q_1^P \in \mathbb{C}^{M \times P}$  form an orthonormal basis of  $\text{span}\{\psi_i\}_{i=1}^P$  and  $\psi_i = Q_1^P \alpha_i$  then

$$[\psi_2 \quad \psi_3 \quad \dots \psi_{P+1}] = Q_1^P \bar{A} Q_1^{P^H} [\psi_1 \quad \psi_2 \quad \dots \psi_P]. \quad (28)$$

$$[\alpha_2 \quad \alpha_3 \quad \dots \alpha_{P+1}] = \bar{A} [\alpha_1 \quad \alpha_2 \quad \dots \alpha_P], \quad (29)$$

This uniquely defines  $\bar{A}$  and  $A := Q_1^P \bar{A} Q_1^{P^H}$ . DMD methods discussed in section 2 generate approximate eigenvectors and eigenvalues of  $A$  in  $\text{span}\{\psi_i\}_{i=1}^{N-1}$  for  $N-1 \leq P$  where  $N$  is the number of snapshots. In exact DMD of Tu et al. (2013), matrix  $A$  is defined as the least square/minimum norm solution connecting the snapshot pairs. The definition of  $A$  changes as new snapshot pairs are added. Here, we interpret  $A$  as a fixed unique linear mapping from  $\text{span}\{\psi_i\}_{i=1}^P$  to itself. This interpretation is same as that by Schmid (2010).

### 2.2.2. Finite precision error analysis of Arnoldi-based DMD variant-1

Due to floating point arithmetic, the computed quantities do not exactly satisfy the theoretical relations. In this section, we first review the numerical stability properties of the QR factorization using Modified Gram-Schmidt (MGS) and classical Arnoldi method using MGS orthogonalization. Then, we perform finite precision error analysis of Arnoldi-based DMD variant-1. Quantities with  $\hat{\phantom{a}}$  over them indicate computed counterparts in finite precision arithmetic and  $\epsilon_m$  denotes machine precision. Then, we compute the estimate of error  $A \hat{V}_1^{N-1} - \hat{V}_1^N \hat{H}_N$ . In deriving error estimate, we only consider real matrices and vectors.  $c_i$ 's are defined as constants that depend on  $M, N$ . i.e.  $c_i := c_i(M, N)$ .

The computed QR factorization of  $Y \in \mathbb{R}^{M \times N}$  using the MGS method is backward-stable and the quality of orthogonality of the computed columns of  $Q$  depends on the condition number of  $Y$  (Higham (2002), Björck and Paige (1992)).

$$Y + \Delta Y_1 = \hat{Q} \hat{R}, \quad \|\Delta Y_1\|_F \leq c_1 \epsilon_m \|Y\|_F \quad (30)$$

$$Y + \Delta Y_2 = \tilde{Q} \hat{R}, \quad \|\Delta Y_2(:, j)\|_2 \leq c_2 \epsilon_m \|a_j\|_2, \quad j = 1 : N \quad (31)$$

$$\|\hat{Q}^T \hat{Q} - I\|_2 \leq c_3 \epsilon_m \kappa_2(Y) + O((\epsilon \kappa_2(Y))^2) \quad (32)$$

where  $\kappa_2(Y)$  is the 2-norm condition number of  $Y$  defined as  $\kappa_2(Y) := \|Y\|_2 \|Y^\dagger\|_2$  and  $\dagger$  denotes the Moore-Penrose pseudo-inverse.  $\tilde{Q}$  is a matrix with orthonormal columns. If reorthogonalization is performed, then the columns of  $\hat{Q}$  are orthonormal up to machine precision (Giraud et al., 2005).

The classical Arnoldi method (algorithm 2) with matrix  $A \in \mathbb{R}^{M \times M}$  is backward stable and the quality of orthogonality of the computed Arnoldi vectors depends on condition number of  $[\hat{v}_1, A\hat{V}_1^N]$  (Drkošová et al., 1995). The below relations were obtained using the above results of modified Gram Schmidt and floating point arithmetic matrix-matrix multiplication of  $A$  and  $\hat{V}_1^N$ .

$$A\hat{V}_1^{N-1} = \hat{V}_1^N \hat{H}_N + E_1, \quad \|E_1\|_2 \leq c_4 \epsilon_m \|A\|_2 \quad (33)$$

$$A\hat{V}_1^{N-1} = \bar{V}_1^N \hat{H}_N + E_2, \quad \|E_2\|_2 \leq c_5 \epsilon_m \|A\|_2 \quad (34)$$

where  $\bar{V}_1^N$  denotes an exact orthonormal matrix in  $\mathbb{R}^{M \times N}$ . Also, the following bound relates the closeness between  $\hat{V}_1^N$  and  $\bar{V}_1^N$

$$\|\hat{V}_1^N - \bar{V}_1^N\|_2 \leq c_6 \epsilon_m \kappa_2([\hat{v}_1, A\hat{V}_1^{N-1}]) \quad (35)$$

assuming  $c_6 \epsilon_m \kappa_2([\hat{v}_1, A\hat{V}_1^{N-1}]) \ll 1$ .

Next, we perform error analysis of Arnoldi-based DMD variant-1 using a similar technique to that used in Drkošová et al. (1995). We obtain the error estimate for  $A\hat{V}_1^{N-1} - \hat{V}_1^N \hat{H}_N$ . We define  $w_j := X_2^{j+1} \hat{\alpha}_{1:j,j}; j = 1, \dots, N-1$ ,  $W_1^{N-1} := [w_1, w_2, \dots, w_{N-1}]$  and  $fl(W_1^{N-1}) := [fl(w_1), fl(w_2), \dots, fl(w_{N-1})]$  where  $fl()$  denotes the result in floating point arithmetic. Since, Arnoldi-based DMD-variant 1 is MGS orthogonalization of  $[\hat{v}_1, fl(W_1^N)]$ ,

$$[\hat{v}_1, fl(W_1^{N-1})] = \hat{V}_1^N \hat{R}_N + [0, E_3], \quad (36)$$

$$\|E_3\|_F \leq c_1 \epsilon_m \|fl(W_1^{N-1})\|_F, \quad (37)$$

where  $\hat{R}_N = [e_1, \hat{H}_N]$  and  $e_1 \in \mathbb{R}^M$  is the first canonical basis vector. We can relate  $fl(W_1^{N-1})$  to  $A\hat{V}_1^{N-1}$  as

$$\|fl(W_1^{N-1}) - A\hat{V}_1^{N-1}\|_F \leq \|fl(W_1^{N-1}) - W_1^{N-1}\|_F + \|A\|_2 \|X_1^{N-1} \hat{\alpha}_1^{N-1} - \hat{V}_1^{N-1}\|_F, \quad (38)$$

where,  $\hat{\alpha}_1^{N-1}$  denotes the submatrix formed by first  $N-1$  rows and columns of  $\hat{\alpha} \in \mathbb{R}^{N \times N}$  matrix. Next, we will show that the terms in right hand side of equation 38 are of order  $\epsilon_m$ . We estimate the difference between  $fl(W_1^{N-1})$  and  $W_1^{N-1}$  using the forward error of floating point matrix-matrix multiplication (Higham, 2002),

$$fl(W_1^{N-1}) = W_1^{N-1} + E_4 \quad (39)$$

$$\|E_4\|_F \leq c_7 \epsilon_m \|X_2^N\|_F \|\hat{\alpha}_1^{N-1}\|_F \leq c_7 \epsilon_m \|A\|_2 \|X_1^{N-1}\|_F \|\hat{\alpha}_1^{N-1}\|_F \quad (40)$$

Now, we write  $E_6 := A\hat{V}_1^{N-1} - \hat{V}_1^N \hat{H}_N$  as a combination of quantities which we can estimate, i.e.

$$A\hat{V}_1^{N-1} - \hat{V}_1^N \hat{H}_N = A(\hat{V}_1^{N-1} - X_1^{N-1} \hat{\alpha}_1^{N-1}) + (W_1^{N-1} - fl(W_1^{N-1})) + (fl(W_1^{N-1}) - \hat{V}_1^N \hat{H}_N). \quad (41)$$

Thus, we have,

$$\|E_6\|_F \leq \|E_3\|_F + \|E_4\|_F + \|A\|_2 \|E_5\|_F, \quad (42)$$

where  $E_5 := \hat{V}_1^{N-1} - X_1^{N-1}\hat{\alpha}_1^{N-1}$ . Using finite precision inner product error estimate for first column of  $E_5$  and  $N-2$  finite precision steps of modified Arnoldi variant-1 in Algorithm. 3 for remaining columns of  $E_5$ , it can be shown that (derivation in Appendix A),

$$\begin{aligned} \|E_5\|_F &\leq C(2\gamma_{2M+1} + \gamma_N\|X_1^{N-1}\|_2 (\|\hat{\alpha}_1^{N-1}\|_2 \|\hat{H}_{N-1}\|_F + \|\hat{\alpha}_1^{N-1}\|_F) + c_7\epsilon_m\|A\|_2\|X_1^{N-1}\|_F\|\hat{\alpha}_1^{N-1}\|_F + \\ &\quad c_1\epsilon_m\|fl(W_1^{N-1})\|_F), \\ C &:= \frac{1}{\sigma_{N-1}([\hat{v}_1, fl(W_1^{N-2})]) - \sqrt{N}c_2\epsilon_m\sigma_1([\hat{v}_1, fl(W_1^{N-2})])} \end{aligned} \quad (43)$$

Note that each term on right hand side of the above equation is of size  $\epsilon_m$ . So, we have

$$\|\hat{\alpha}_1^{N-1}\|_F \leq \|X_1^{N-1}\|_2 \sqrt{N} + O(\epsilon_m), \quad (44)$$

$$\|\hat{H}_{N-1}\|_F \leq \|\hat{H}_N\|_2 \leq N\|A\|_2 + O(\epsilon_m), \quad (45)$$

$$\|fl(W_1^{N-1})\|_F \leq \sqrt{N}\|A\|_2 + O(\epsilon_m). \quad (46)$$

Using the above estimates of  $\|\hat{\alpha}_1^{N-1}\|_F$ ,  $\|\hat{H}_{N-1}\|_F$  and  $\|fl(W_1^{N-1})\|_F$  in equations 37, 40 and 43,

$$\|E_3\|_F \leq c_1\epsilon_m \sqrt{N}\|A\|_2 + O(\epsilon_m^2), \quad (47)$$

$$\|E_4\|_F \leq c_7\epsilon_m\|A\|_2\kappa_2(X_1^{N-1}), \quad (48)$$

$$\|E_5\|_F \leq C(2\gamma_{2M+1} + \gamma_N N\kappa_2(X_1^{N-1}) (\|A\|_2 + 1) + c_7\epsilon_m\|A\|_2\kappa_2(X_1^{N-1}) + c_1\epsilon_m \sqrt{N}\|A\|_2) + O(\epsilon_m^2), \quad (49)$$

$$\begin{aligned} \|A\hat{V}_1^{N-1} - \hat{V}_1^N\hat{H}_N\|_F &\leq c_1\epsilon_m \sqrt{N}\|A\|_2 + c_7\epsilon_m\|A\|_2\kappa_2(X_1^{N-1}) + \\ &\quad C\|A\|_2(2\gamma_{2M+1} + \gamma_N N\kappa_2(X_1^{N-1}) (\|A\|_2 + 1) + c_7\epsilon_m\|A\|_2\kappa_2(X_1^{N-1}) + c_1\epsilon_m \sqrt{N}\|A\|_2) + O(\epsilon_m^2). \end{aligned} \quad (50)$$

From equation 50 we can see that the size of  $A\hat{V}_1^{N-1} - \hat{V}_1^N\hat{H}_N$  is of order  $\epsilon_m\kappa_2(X_1^{N-1})$ . Consequently the error in projected  $A$  onto the span of columns of  $\hat{V}_1^N$  i.e.  $\hat{V}_1^{N-1H}A\hat{V}_1^{N-1} - \hat{H}_{N-1}$  is also bounded by  $O(\epsilon_m\kappa_2(X_1^{N-1}))$ . So, the obtained upper Hessenberg matrix is close to the projected  $A$  if the condition number of the snapshots is sufficiently less than  $O(\epsilon_m^{-1})$ . It can be seen from the error analysis that it was the matrix multiplication  $X_2^N\alpha_1^{N-1}$  and the computation of  $\alpha$  matrix that led to error being proportional to  $\kappa_2(X_1^{N-1})$ . The classical Arnoldi method (algorithm 2) does not have this dependency (see equation 33) as it involves matrix multiplication of  $A$  with an orthonormal matrix  $V_1^{N-1}$  which is backward stable. Also, the quality of computed orthogonal vectors  $\hat{V}_1^N$  computed by algorithm 3 depends on condition number of  $fl(W_1^{N-1})$  and not that of the snapshot matrix. The computed Arnoldi vectors can be made orthogonal to machine precision either by using MGS with re-orthogonalization (Giraud et al., 2005) or by replacing the orthogonalization kernel with Householder algorithm instead of MGS (Walker, 1988). The error in the factorization of  $X_1^{N-1}$  into  $\hat{V}_1^{N-1}$  and  $\alpha_1^{N-1}$ ,  $X_1^{N-1}\alpha_1^{N-1} - V_1^{N-1}$  is also of order  $\epsilon_m\kappa_2(X_1^{N-1})$ . This can be improved by factorizing  $X_1^{N-1}$  into  $V_1^{N-1}$  and a matrix similar to inverse of  $\alpha_1^{N-1}$  matrix in a backward stable manner and then using these two matrices to compute  $\hat{A}v_j$ . This forms the basis of the next method which we call FOADMD algorithm.

```

1: Construct initial vector  $v_1$  from the first snapshot.  $v_1 := \frac{\psi_1}{\|\psi_1\|_2}$ 
2:  $\beta_{1,1} = \|\psi_1\|_2$ 
3: for  $j=1$  to  $N-1$  do
4:    $Av_j = \frac{1}{\beta_{j,j}} (\psi_{j+1} - \sum_{k=1}^{j-1} \beta_{k,j} Av_k)$  //Step replacing  $Av_j$ 
5:    $w = Av_j$ 
6:   for  $i=1$  to  $j$  do
7:      $h_{i,j} = (w, v_i)$ 
8:      $w = w - h_{i,j} v_i$ 
9:   end for
10:   $h_{j+1,j} = \|w\|_2; v_{j+1} = \frac{w}{h_{j+1,j}}$ 
11:   $\beta_{1,j+1} = h(1, 1 : j) \beta(1 : j, j)$ 
12:  for  $i=2$  to  $j+1$  do
13:     $\beta_{i,j+1} = h(i, i-1 : j) \beta(i-1 : j, j)$ 
14:  end for
15: end for

```

**Algorithm 5:** Modified FOA method.

### 2.3. Proposed FOADMD algorithm

Algorithm 5 forms the kernel of the proposed FOADMD algorithm. In algorithm 5, we still use the property that  $\text{span}\{\psi_1, \dots, \psi_j\}$  is the same as the span of  $\text{span}\{v_1, \dots, v_j\}$ . But instead of forming  $v_j$  as a linear combination of vectors  $\{\psi_i\}_{i=1}^j$ , we express  $\psi_j$  as a linear combination of  $\{v_i\}_{i=1}^j$ . Given the previously evaluated submatrix  $\beta_1^j$ , we have

$$\psi_j = \sum_{i=1}^j \beta_{i,j} v_i. \quad (51)$$

Then, this relation is used to compute  $Av_j$  in the next step as follows.

$$A\psi_j = \psi_{j+1} = \sum_{i=1}^j \beta_{i,j} Av_i \quad (52)$$

Rearranging equation 52, we obtain a recursive relation to compute  $Av_j$  using previously computed  $\{Av_i\}_{i=1}^{j-1}$  as

$$Av_j = \frac{1}{\beta_{j,j}} \left( \psi_{j+1} - \sum_{i=1}^{j-1} \beta_{i,j} Av_i \right). \quad (53)$$

Using the computed  $j^{th}$  column of  $\bar{H}_N$ ,  $\beta$  and observable vector  $\psi_{j+1}$ , we can compute the  $(j+1)^{th}$  column of  $\beta$  using the relation

$$Av_j = \sum_{i=1}^{j+1} h_{i,j} v_i. \quad (54)$$

Substituting equation 54 for  $Av_j$  and  $Av_i$  in equation 53,

$$\psi_{j+1} = \sum_{i=1}^{j+1} \beta_{j,j} h_{i,j} v_i + \sum_{k=1}^{j-1} \beta_{k,j} \sum_{i=1}^{k+1} h_{i,k} v_i. \quad (55)$$

Rearranging, we have

$$\psi_{j+1} = \sum_{k=1}^j h_{1,k} \beta_{k,j} v_1 + \sum_{i=2}^{j+1} \sum_{k=i-1}^j h_{i,k} \beta_{k,j} v_i. \quad (56)$$

Since  $\psi_{j+1} = \sum_{i=1}^{j+1} \beta_{i,j+1} v_i$ , we have

$$\begin{aligned}\beta_{1,j+1} &= \sum_{k=1}^j h_{1,k} \beta_{k,j}, \\ \beta_{i,j+1} &= \sum_{k=i-1}^j h_{i,k} \beta_{k,j}; \quad i = 2, \dots, j+1.\end{aligned}\tag{57}$$

The DMD eigenvalues and eigenvectors are then obtained from the eigenvalues and eigenvectors of  $H_{N-1}$  in a manner similar to Arnoldi-based DMD variant-1. Algorithm 6 summarizes the FOADMD method.

- 1: Form snapshot matrix  $X_1^N$
- 2: Compute  $V_1^{N-1}$  and  $H_{N-1}$  from  $X_1^N$  using modified FOA method.
- 3: Compute eigenvalues  $\{\lambda_i\}_{i=1}^{N-1}$  and eigenvectors  $\{z_i\}_{i=1}^{N-1}$  of  $H_{N-1}$
- 4: DMD eigenvalues are  $\{\lambda_i\}_{i=1}^{N-1}$  and DMD eigenvectors are  $\{V_1^{N-1} z_i\}_{i=1}^{N-1}$

**Algorithm 6:** Proposed FOADMD method for sequence of snapshots.

Even though FOADMD (algorithm 5) is theoretically equivalent to Arnoldi-based variant-1 (algorithm 3), the accuracy obtained in floating point arithmetic is different, and is analyzed in next section. In fact, algorithm 5 factorizes  $X_1^N$  into  $V_1^N$  and  $\beta_1^N$  which has smaller error when compared to the factorization of  $V_1^N$  into  $X_1^N$  and  $a_1^N$  by algorithm 3, as shown in next section.

### 3. Remarks on FOADMD

We will assume that the eigenvectors of  $H_{N-1}$  matrix are linearly independent.

#### 3.1. Finite precision error analysis of FOADMD algorithm

From the backward stability result of MGS in equation 30, we have

$$\begin{aligned}[\hat{v}_1, L_1^{N-1}] &= \hat{V}_1^N \hat{R}_N + E_7, \\ \|E_7\|_F &\leq c_7 \epsilon_m \|L_1^{N-1}\|_F,\end{aligned}\tag{58}$$

where  $L_1^{N-1} := [\hat{A}v_1, \dots, \hat{A}v_{N-1}]$  is the computed analogue of  $Av_j$ . We want to examine how close  $L_1^{N-1}$  is to  $A\hat{V}_1^{N-1}$ . Assuming  $\hat{\beta}_1^{N-1}$  to be invertible,

$$\begin{aligned}\|L_1^{N-1} - A\hat{V}_1^{N-1}\|_F &= \left\| \left[ L_1^{N-1} \hat{\beta}_1^{N-1} - A\hat{V}_1^{N-1} \hat{\beta}_1^{N-1} \right] \hat{\beta}_1^{N-1} \right\|_F \\ &= \left\| \left[ L_1^{N-1} \hat{\beta}_1^{N-1} - X_2^N + A \left( X_1^{N-1} - \hat{V}_1^{N-1} \hat{\beta}_1^{N-1} \right) \right] \hat{\beta}_1^{N-1} \right\|_F \\ &\leq \|L_1^{N-1} \hat{\beta}_1^{N-1} - X_2^N\|_F \|\hat{\beta}_1^{N-1}\|_2 + \|A\|_2 \|X_1^{N-1} - \hat{V}_1^{N-1} \hat{\beta}_1^{N-1}\|_F \|\hat{\beta}_1^{N-1}\|_2.\end{aligned}\tag{59}$$

Next, we show that the terms in right hand side of inequality are of  $O(\epsilon_m)$ .  $\|X_2^N - L_1^{N-1} \hat{\beta}_1^{N-1}\|_F$  is estimated using the expression used to compute  $L(:, j)$ .

$$L(:, j) = fl \left( \frac{1}{\hat{\beta}_{j,j}} \left[ \psi_{j+1} - \sum_{k=1}^{j-1} \beta_{k,j} L(:, k) \right] \right); j = 1, \dots, N-1\tag{60}$$

The obtained estimate of  $E_8 := X_2^N - L_1^{N-1}\hat{\beta}_1^{N-1}$  from forward error of floating point arithmetic matrix-matrix multiplication result (Higham, 2002) is

$$\|E_8\|_F \leq \gamma_{N+1} \left( \|X_2^N\|_F + \|L_1^{N-1}\|_2 \|\hat{\beta}_1^{N-1}\|_F \right). \quad (61)$$

Next, we find the error in factorization of  $X_1^{N-1}$  into  $\hat{V}_1^{N-1}$  and  $\hat{\beta}_1^{N-1}$  obtained from algorithm 5. Let  $E_9 := X_1^{N-1} - \hat{V}_1^{N-1}\hat{\beta}_1^{N-1}$ . Then, an estimate for the first column of  $E_9$ , i.e.  $E_9(1, :)$  can be obtained using floating point arithmetic model (Higham, 2002), as

$$\begin{aligned} E_9(1, :) &= \hat{v}_1 \hat{\beta}_{1,1} - \psi_1, \\ \hat{\beta}_{1,1} &= \text{fl}(\psi_1^H \psi_1), \quad \hat{v}_1 = \text{fl}\left(\frac{\psi_1}{\hat{\beta}_{1,1}}\right), \\ E_9(1, :) &= \psi_1 \delta, \end{aligned} \quad (62)$$

where  $|\delta| \leq \epsilon_m$ . For an estimate of the second to  $N - 1$  columns of  $E_9$ , we use equations 58 and 61.

$$\begin{aligned} X_2^{N-1} &= \hat{L}_1^{N-2} \hat{\beta}_1^{N-2} + E_8(:, 1 : N - 2) \\ &= \hat{V}_1^{N-1} \hat{H}_{N-1} \hat{\beta}_1^{N-2} + E_7 \hat{\beta}_1^{N-2}(:, 1 : N - 2) + E_8(:, 1 : N - 2) \\ &= \hat{V}_1^{N-1} \hat{\beta}_{1:N-1, 2:N} - 1 + \hat{V}_1^{N-1} [\hat{H}_{N-1} \hat{\beta}_1^{N-2} - \hat{\beta}_{1:N-1, 2:N-1}] + \\ &\quad E_7(:, 1 : N - 2) \hat{\beta}_1^{N-2} + E_8(:, 1 : N - 2) \end{aligned} \quad (63)$$

$$\|E_9\|_F \leq \epsilon_m + \gamma_N \sqrt{N} \|\hat{H}_N\|_F \|\hat{\beta}_1^{N-1}\|_F + \|E_7\|_F \|\hat{\beta}_1^{N-1}\|_2 + \|E_8\|_F. \quad (64)$$

From equations 64 and 62, we have

$$\begin{aligned} \|\hat{\beta}_1^{N-1}\|_F &\leq \sqrt{N} \|X_1^{N-1}\|_2 + O(\epsilon_m), \\ \|\hat{\beta}_1^{N-1}\|_F &\leq \sqrt{N} \|X_1^{N-1}\|_2 + O(\epsilon_m). \end{aligned} \quad (65)$$

We have now shown that the right hand side terms of equation 59 are of  $O(\epsilon_m)$ . Therefore, we have the following estimate for  $E_7$ ,

$$\begin{aligned} \|L_1^{N-1}\|_F &= \sqrt{N} \|A\|_2 + O(\epsilon_m), \\ \|E_7\|_F &\leq c_7 \epsilon_m \|A\|_2 \sqrt{N} + O(\epsilon_m^2). \end{aligned} \quad (66)$$

Also, using the MGS result that relates  $\|\hat{H}_N\|_F$  and  $\|[\hat{v}_1, L_1^{N-1}]\|_F$  from Higham (2002), we can bound  $\|\hat{H}_N\|_F$  with  $\|A\|_2$  as

$$\begin{aligned} \|\hat{H}_N\|_F &\leq \sqrt{N} \|L_1^{N-1}\|_F + O(\epsilon_m), \\ &\leq N \|A\|_2 + O(\epsilon_m). \end{aligned} \quad (67)$$

Substituting equation 66 in 61, the estimates for error  $X_2^N - L_1^{N-1}\hat{\beta}_1^{N-1}$  and  $X_1^N - \hat{V}_1^N\hat{\beta}_1^N$  become

$$\begin{aligned} \|E_8\|_F &\leq \gamma_{N+1} \left( \|A\|_2 \|X_1^{N-1}\|_F + \sqrt{N} \|A\|_2 \|X_1^{N-1}\|_F \right) + O(\epsilon_m^2), \\ \|E_9\|_F &\leq \epsilon_m \|X_1^{N-1}\|_2 + \gamma_N N^2 \|A\|_2 \|X_1^{N-1}\|_2 + \|E_7\|_F \|X_1^{N-1}\|_2 + \|E_8\|_F. \end{aligned} \quad (68)$$

Next, we estimate the error  $E_{10} := A \hat{V}_1^{N-1} - \hat{V}_1^N \hat{H}_N$ . Multiplying equation 58 by  $\hat{\beta}_1^{N-1}$ , we have

$$\hat{L}_1^{N-1} \hat{\beta}_1^{N-1} = \hat{V}_1^N \hat{H}_N \hat{\beta}_1^{N-1} + E_7 \hat{\beta}_1^{N-1}. \quad (69)$$

Using equations 61 and 64, we have

$$X_2^N - \hat{V}_1^N \hat{H}_N \hat{\beta}_1^{N-1} = E_7 \hat{\beta}_1^{N-1} + E_8, \quad (70)$$

$$AX_1^{N-1} - \hat{V}_1^N \hat{H}_N \hat{\beta}_1^{N-1} = E_7 \hat{\beta}_1^{N-1} + E_8, \quad (71)$$

$$A \hat{V}_1^{N-1} \hat{\beta}_1^{N-1} - \hat{V}_1^N \hat{H}_N \hat{\beta}_1^{N-1} = E_7 \hat{\beta}_1^{N-1} + E_8 - AE_9. \quad (72)$$

Assuming  $\hat{\beta}_1^{N-1}$  to be invertible, we can obtain estimate for  $E_{10}$  as

$$\begin{aligned} A \hat{V}_1^{N-1} - \hat{V}_1^N \hat{H}_N &= E_7 - E_8 \hat{\beta}_1^{N-1} - AE_9(:, 1 : N-1) \hat{\beta}_1^{N-1}, \\ \|E_{10}\|_F &\leq \|E_7\|_F + \|E_8\|_F \|\hat{\beta}_1^{N-1}\|_2 + \|A\|_2 \|E_9\|_F \|\hat{\beta}_1^{N-1}\|_2. \end{aligned} \quad (73)$$

Using equation 66 and 68 in the above equation, we get

$$\|E_{10}\|_F \leq O(\epsilon_m \|A\|_2) + O(\epsilon_m \|A\|_2 \kappa_2(X_1^{N-1})) + O(\epsilon_m \|A\|_2^2 \kappa_2(X_1^{N-1})) + O(\epsilon_m^2). \quad (74)$$

Equation 74 indicates that the difference between the projected  $A$  and the computed upper Hessenberg matrix  $\hat{H}_{N-1}$  is  $O(\epsilon_m \kappa_2(X_1^{N-1}))$ . So, the quality of computed Hessenberg matrices decreases as the condition number of the snapshot matrix increases. From equation 68, it can be seen that the quality of factorization of  $X_1^{N-1}$  into  $\hat{V}_1^{N-1}$  and  $\hat{\beta}_1^{N-1}$  is close to machine precision. This is an improvement when compared to Arnoldi-based DMD variant-1 where the error in factorization of  $X_1^{N-1}$  into  $\hat{V}_1^{N-1}$  and  $\hat{\alpha}_1^{N-1}$  is  $O(\epsilon_m \kappa_2(X_1^{N-1}))$ . However, the implementations of both Arnoldi-based DMD variant-1 and FOADMD have error  $\hat{V}_1^{N-1H} A \hat{V}_1^{N-1} - \hat{H}_{N-1}$  that depend on quantities of  $O(\epsilon_m \kappa_2(X_1^{N-1}))$ .

Next, we perform finite precision error analysis of SVD based DMD methodology of Schmid (2010). The computed SVD has the property (Golub and Van Loan, 2012),

$$\begin{aligned} X_1^{N-1} + E &= (\hat{U} + \delta \hat{U}) \hat{S} (\hat{W} + \delta \hat{W})^H, \\ \|E\|_2 &\leq p_1 \epsilon_m \|X_1^{N-1}\|_2, \\ \|\delta \hat{U}\|_2 &\leq p_2 \epsilon_m, \quad \|\delta \hat{V}\|_2 \leq p_3 \epsilon_m. \end{aligned} \quad (75)$$

where  $p_1, p_2, p_3$  are polynomials of reasonable degree in the matrix dimensions of  $X_1^{N-1}$ . First, we estimate how close is  $A \hat{U} \hat{S} \hat{W}^H$  to  $X_2^N$ .

$$\begin{aligned} A \hat{U} \hat{S} \hat{W}^H &= A (X_1^{N-1} + E - \delta \hat{U} \hat{S} \delta \hat{W}^H - \hat{U} \hat{S} \delta \hat{W}^H) \\ &= X_2^N + A (E - \delta \hat{U} \hat{S} (\hat{W} + \delta \hat{W})^H - \hat{U} \hat{S} \delta \hat{W}^H) \end{aligned} \quad (76)$$

Multiplying the above equation by  $\hat{W} \hat{S}^{-1}$  from the right, we have

$$A \hat{U} = X_2^N \hat{W} \hat{S}^{-1} + A (E - \delta \hat{U} \hat{S} (\hat{W} + \delta \hat{W})^H - \hat{U} \hat{S} \delta \hat{W}^H) \hat{W} \hat{S}^{-1} \quad (77)$$

Multiplying the above equation by  $U^H$  on left and accounting for the error in matrix-matrix multiplication,

$$\begin{aligned} U^H A U - fl(U^H X_2^N \hat{W} \hat{S}^{-1}) &= [U^H X_2^N \hat{W} \hat{S}^{-1} - fl(U^H X_2^N \hat{W} \hat{S}^{-1})] + \\ &\quad [U^H A (E - \delta \hat{U} \hat{S} (\hat{W} + \delta \hat{W})^H - \hat{U} \hat{S} \delta \hat{W}^H) \hat{W} \hat{S}^{-1}] \end{aligned} \quad (78)$$

Observe that each of the two bracketed terms in right hand side is of size  $O(\epsilon_m \kappa_2(X_1^N))$ . So, the error in the computed projection of  $A$  is  $O(\epsilon_m \kappa_2(X_1^N))$  even using the SVD approach. So, this dependency of the computed projection of  $A$  is essentially because we work with snapshots that are generated as a result of the action of  $A$  on vectors rather than the mapping  $A$  itself.

Note that from equation 71, choosing  $X_1^{N-1}$  as the basis of the eigenvector and  $\hat{V}_1^{N-1}$  as the basis to perform orthogonal projection a backward stable projection of  $A$  can be obtained.

$$\hat{V}_1^{N-1H} A X_1^{N-1} - \hat{H}_{N-1} \hat{\beta}_1^{N-1} = \hat{V}_1^{N-1H} (E_7 \hat{\beta}_1^{N-1} - E_8) \quad (79)$$

The generalized eigenvalue problem  $\hat{H}_{N-1} \hat{\beta}_1^{N-1} z = \lambda \hat{\beta}_1^{N-1} z$ , turns out to be extremely ill-conditioned. However, the eigenvalue problem of  $\hat{H}_{N-1}$  turns out to be better conditioned, even though the projection of  $A$  that lead to  $\hat{H}_{N-1}$  is not backward stable as can be seen in equation 74.

### 3.2. Relation to DMD methods based on rank truncated SVD

From equation 72, note that the error in  $A \hat{V}_1^{N-1} \hat{\beta}_1^{N-1} - \hat{V}_1^N \hat{H}_N \hat{\beta}_1^{N-1}$  is small and does not depend on condition number of snapshots of observables. It is in the following equation when we multiply by inverse of  $\hat{\beta}_1^{N-1}$  that we introduce dependence of  $A \hat{V}_1^{N-1} - \hat{V}_1^N \hat{H}_N$  on the condition number of snapshots. If the smallest singular value of  $\hat{\beta}$  is very close to 0, then  $\|\hat{\beta}^{-1}\|_2$  is very large thereby indicating larger error  $A \hat{V}_1^{N-1} - \hat{V}_1^N \hat{H}_N$  and  $\hat{V}_1^{N-1H} A \hat{V}_1^{N-1} - \hat{H}_{N-1}$ . So, the computed projection of  $A$  onto the Krylov subspace will have large error. However, we can choose a subspace of the Krylov subspace on which we can more accurately compute the projection of  $A$ .

Now, we multiply the last equation in equation 72 not by the inverse of  $\hat{\beta}_1^{N-1}$  but by the pseudo-inverse of matrix  $\hat{\beta}_1^{N-1}$  which is close to  $\hat{\beta}_1^{N-1-1}$ . The matrix  $\hat{\beta}_1^{N-1}$  is chosen such that its pseudo-inverse has a 2-norm that is much smaller than the inverse of  $\hat{\beta}_1^{N-1}$ . Then, the error in the resulting relation should be much smaller than that given by equation 74. Choosing  $\hat{\beta}_1^{N-1}$  as the rank truncated SVD of  $\hat{\beta}_1^{N-1}$  and assuming  $\hat{\beta}_1^{N-1}$  to be full rank, we have

$$\hat{\beta}_1^{N-1} = U \Sigma W^H, \quad (80)$$

$$\hat{\beta}_1^{N-1} = U_r \Sigma_r W_r^H, \quad (81)$$

where  $U, \Sigma, W$  are the left singular vectors, matrix of singular values, right singular vectors respectively,  $U_r$  represents that first 'r' columns of matrix  $U$ ,  $W_r$  is the first 'r' rows of matrix  $W$  and  $\Sigma_r$  is the  $r \times r$  sub-matrix of  $\Sigma$ . The pseudo-inverse  $\hat{\beta}_1^{N-1\dagger}$  of  $\hat{\beta}_1^{N-1}$  is then

$$\hat{\beta}_1^{N-1\dagger} = W_r \Sigma_r^{-1} U_r^H. \quad (82)$$

Multiplying equation 72 by pseudo-inverse  $\hat{\beta}_1^{N-1\dagger}$  and using equation 81, we have

$$A \hat{V}_1^{N-1} U_r U_r^H - \hat{V}_1^N \hat{H}_N U_r U_r^H = E_7 U_r U_r^H - E_8 \hat{\beta}_1^{N-1\dagger} - A E_9 \hat{\beta}_1^{N-1\dagger}, \quad (83)$$

$$A \hat{V}_1^{N-1} U_r - \hat{V}_1^N \hat{H}_N U_r = E_7 U_r - E_8 \hat{\beta}_1^{N-1\dagger} U_r - A E_9 \hat{\beta}_1^{N-1\dagger} U_r, \quad (84)$$

$$\|A \hat{V}_1^{N-1} U_r - \hat{V}_1^N \hat{H}_N U_r\|_2 \leq \|E_7\|_2 + \|E_8\|_2 \|\hat{\beta}_1^{N-1\dagger}\|_2 + \|A\|_2 \|E_9\|_2 \|\hat{\beta}_1^{N-1\dagger}\|_2. \quad (85)$$

The columns of  $\hat{V}_1^{N-1}U_r$  represent a subspace of the Krylov subspace (equation 4). The computed projection of  $A$  onto the subspace formed by the columns of  $\hat{V}_1^{N-1}U_r$  is then  $U_r^H \hat{H}_{N-1} U_r$ . Since,  $\|\hat{\beta}_1^{N-1}\|_2$  is much less than  $\|X_1^{N-1}\|_2$ , equation 85 tells us that the error in the computed projection of  $A$  onto subspace  $V_1^{N-1}U_r$  is smaller than that onto  $V_1^{N-1}$ . A similar argument explains the better accuracy of computed projection of SVD based DMD methods with rank truncation. Also, the DMD eigenvalue  $\lambda$  of  $U_r^H \hat{H}_{N-1} U_r$  and DMD eigenvector  $V_1^{N-1}U_r z$ , where  $z$  is the eigenvector corresponding to  $\lambda$ , are nearly the same as the ones that one would obtain using DMD with rank truncated SVD Schmid (2010).

However, as we will see in our numerical experiment, even though the floating point error in the projected  $A$  is smaller onto the subspace of  $\mathbb{C}^M$  formed by the range of  $V_1^{N-1}U_r$ , the accuracy of the computed DMD eigenvectors and eigenvalues for the dominant eigenvalues are nearly the same when projecting the mapping  $A$  onto the Krylov subspace (span of columns of  $V_{N-1}$ ).

### 3.3. Error in DMD eigenvectors and DMD eigenvalues

To obtain the exact eigenvectors and eigenvalues of  $A$ , we need to use  $P+1$  ( $P$  is defined in section 2.2.1) snapshots. If we use  $N$  snapshots and perform FOADMD, we obtain approximate eigenvectors and eigenvalues of  $A$  (also called DMD eigenvectors and DMD eigenvalues). In exact arithmetic, using matrix  $\bar{H}_N$  and the eigenvector  $z_i$  it is possible to obtain error estimates associated with DMD eigenvalues and DMD eigenvectors (Saad, 2011) in  $\ell^2$  norm by using the relation

$$\|AV_1^{N-1}z_i - \lambda_i V_1^{N-1}z_i\|_2 = \|h_{N,N-1}v_N e_{N-1}^H z_i\|_2. \quad (86)$$

By monitoring the value of  $\|h_{N,N-1}v_N e_{N-1}^H z_i\|_2$  it is possible to monitor the accuracy of DMD eigenvector and eigenvalue pairs. This can be used to device effective stopping criterion for DMD. It can be seen that  $\beta_{N,N}$  is the residual associated with the orthogonal projection of last snapshot onto the span of previous snapshots. Let  $\varphi_j := V_1^{N-1}z_j$ ;  $j = 1, \dots, N-1$ . Since, we have assumed that the DMD eigenvectors are linearly independent,  $\text{span}\{\varphi_i\}_{i=1}^{N-1}$  is same as  $\chi_1^{N-1}$ . So, we should be able to reconstruct atleast  $N-1$  snapshots using  $\{\varphi_j\}_{j=1}^{N-1}$  exactly (Rowley et al., 2009).

Suppose  $\psi = \sum_{j=1}^{N-1} c_j \varphi_j$ . Then, say we approximate  $A\psi$  as  $\sum_{j=1}^{N-1} \lambda_j c_j \varphi_j$ . The error involved in this approximation can be obtained as follows

$$\begin{aligned} A\psi - \sum_{j=1}^{N-1} \lambda_j c_j \varphi_j &= \sum_{j=1}^{N-1} c_j (A\varphi_j - \lambda_j \varphi_j) \\ &= \sum_{j=1}^{N-1} c_j (h_{N,N-1}v_N e_{N-1}^H z_j) = h_{N,N-1} \left( \sum_{j=1}^{N-1} c_j e_{N-1}^H z_j \right) v_N, \end{aligned} \quad (87)$$

$$\|A\psi - \sum_{j=1}^{N-1} \lambda_j c_j \varphi_j\|_2 = |h_{N,N-1}| \left| \sum_{j=1}^{N-1} c_j e_{N-1}^H z_j \right|. \quad (88)$$

$\psi = \sum_{j=1}^{N-1} c_j \varphi_j$  can be written in matrix form as  $\psi = [\varphi][c]$  where  $[\varphi]$  is matrix formed by stacking  $\varphi_j$  as columns and  $[c]$  is the vector of coefficients. i.e.  $[\varphi] = [\varphi_1 \quad \dots \quad \varphi_{N-1}]$  and  $[c] = [c_1 \quad \dots \quad c_{N-1}]^H$ . Let  $[z] := [z_1 \quad \dots \quad z_{N-1}]$ .

Then, we have

$$\begin{aligned}\psi &= V_1^{N-1}[z][c], \\ \psi &= V_1^{N-1}[\tilde{c}] \quad (\tilde{c} := [z][c]).\end{aligned}\tag{89}$$

Suppose  $h_{N,N-1}$  is not 0. Then,  $\|A\psi - \sum_{j=1}^{N-1} \lambda_j c_j \varphi_j\|_2$  is 0 if  $\sum_{j=1}^{N-1} c_j e_{N-1}^H z_j$  is 0. i.e. the last entry in the vector  $[\tilde{c}]$  should be 0 or equivalently,  $\psi = V_1^{N-2}[\tilde{c}]$  where  $[\tilde{c}] = [\tilde{c}_1 \dots \tilde{c}_{N-2}]^T$ . Therefore the approximation  $\sum_{j=1}^{N-1} \lambda_j c_j \varphi_j$  to  $A\psi$  is exact if atleast one of the below conditions are satisfied.

1.  $\psi$  is in the range of  $V_{N-2}$ .
2.  $h_{N,N-1} = 0$ . i.e. if the last snapshot can be written as linear combination of the previous snapshots.

DMD generates an interpolant through the snapshot vectors. The interpolant can be defined as

$$\begin{aligned}I^N\psi(t) &:= \sum_{j=1}^{N-1} e^{\omega_j t} d_j \varphi_j, \\ I^N\psi_k &:= I^N\psi(t_k),\end{aligned}\tag{90}$$

where  $\omega_j := \ln(\lambda_j)/\Delta t$ ,  $\Delta t$  is the time spacing between the snapshots,  $t_k := (k-1)\Delta t$  and  $\psi_1 = \sum_{j=1}^{N-1} d_j \varphi_j$ . Equation 88 implies that snapshots  $\psi_1$  to  $\psi_{N-2}$  can always be exactly reconstructed from the DMD eigenmodes and DMD eigenvalues. i.e.

$$\psi_k = I^N\psi_k \quad k = 1, \dots, N-1\tag{91}$$

and the error associated with reconstruction of  $I^N\psi_{N-1}$  is

$$\|I^N\psi_N - \psi_N\|_2 = |h_{N,N-1}| \sum_{j=1}^{N-1} d_j \lambda_j^{N-2} e_{N-1}^H z_j.\tag{92}$$

Suppose, we use  $P+1$  snapshots in FOADMD process starting from snapshot  $\psi_1$ , then DMD eigenvectors and eigenvalues are the exact eigenvectors of  $A$  because  $h_{P+1,P}$  would turn out to be 0. All  $P+1$  snapshots can be constructed exactly using DMD eigenvectors and DMD eigenvalues. Now, if we use  $I^P\psi(t)$  to predict the observable vectors at future times, the error in the prediction is an indication of how close are these DMD modes and eigenvalues to Koopman modes and eigenvalues.

Next, we investigate how close the computed error indicator  $\hat{h}_{N,N-1} \hat{v}_N e_{N-1}^H \hat{z}_i$  is to the actual error using the finite precision results derived in previous section for FOADMD. From equation 72 and assuming  $\hat{\beta}_1^{N-1}$  to be full rank, we have

$$A \hat{V}_1^{N-1} \hat{\beta}_1^{N-1} y - \hat{V}_1^N \hat{H}_N \hat{\beta}_1^{N-1} y = E_7 \hat{\beta}_1^{N-1} y - E_8 y - A E_9(:, 1:N-1) y,\tag{93}$$

$$\hat{\beta}_1^{N-1} y = z,\tag{94}$$

where  $\lambda, z$  is an exact eigenvalue eigenvector pair of  $\hat{H}_{N-1}$ . Here, we assume for simplicity that the  $y$  is the exact solution of  $\hat{\beta}_1^{N-1} y = z$  and  $z$  is the exact eigenvector of  $\hat{H}_{N-1}$ . Then, the accuracy of the eigenvalue eigenvector pair is

$$A \hat{V}_1^{N-1} z - \lambda \hat{V}_1^{N-1} z = \hat{h}_{N,N-1} \hat{v}_N e_{N-1}^H z + E_7 \hat{\beta}_1^{N-1} y - E_8 y - A E_9(:, 1:N-1) y\tag{95}$$

The above equation tells us that the computed error indicator  $\hat{h}_{N,N-1}\hat{v}_N e_{N-1}^H z$  is a good estimate of the actual error  $A\hat{V}_1^{N-1}z - \lambda\hat{V}_1^{N-1}z$  if the magnitude of  $y$  obtained from solving equation 94 is small. This is essentially the same as saying that the component of  $z$  along the left singular vectors corresponding to near zero singular values of  $\hat{\beta}_1^{N-1}$  is small.

Suppose, we use FOADMD with rank truncation, the error indicator for the DMD eigenvectors and DMD eigenvalues can be obtained as follows. From rank truncated version of FOADMD (equation 84) in exact arithmetic,

$$\begin{aligned} AV_1^{N-1}U_r z - \lambda V_1^{N-1}U_r z &= V_1^{N-1}(I - U_r U_r^H)H_{N-1}U_r z + h_{N,N-1}v_N e_{N-1}^H U_r z \\ \|AV_1^{N-1}U_r z - \lambda V_1^{N-1}U_r z\|_2 &= \|V_1^{N-1}(I - U_r U_r^H)H_{N-1}U_r z + h_{N,N-1}v_N e_{N-1}^H U_r z\|_2 \\ \|AV_1^{N-1}U_r z - \lambda V_1^{N-1}U_r z\|_2 &= \left\| \begin{bmatrix} (I - U_r U_r^H)H_{N-1} \\ h_{N,N-1}e_{N-1}^H \end{bmatrix} U_r z \right\|_2 \end{aligned} \quad (96)$$

The computed error indicator  $\left\| \begin{bmatrix} (I - U_r U_r^H)H_{N-1} \\ h_{N,N-1}e_{N-1}^H \end{bmatrix} U_r z \right\|_2$  will be very close to the actual error in eigenvalue-eigenvector pair as the backward error in equation 85 is small and controlled by  $\|\hat{\beta}_1^{N-1}\|_2$  rather than  $\|\hat{\beta}_1^{N-1}\|_2$ .

### 3.4. Implementation aspects

The method stops if linearly dependent snapshots are present. i.e. say  $\psi_{j+1}$  can be expressed as a linear combination of  $\{\psi_1, \dots, \psi_j\}$ . Then, in  $j^{th}$  step of Arnoldi method,  $h_{j+1,j}$  is 0. The Galerkin method with the previously computed  $v_i$ 's will give exact eigenvectors and eigenvalues associated with the linear mapping  $A$ . The operation count of the modified FOA method (without re-orthogonalization) is  $3Mr^2 - Mr + M + r(r-1)(r+4)/3$  where  $r$  is the rank of snapshot matrix. The FOADMD algorithm can be easily parallelized. The snapshot data can be partitioned row-wise among different processors. The only computational kernels that have to be parallelized are vector additions and dot products. Figs. 1a and 1b show strong scaling for the FOADMD algorithm with re-orthogonalization on Minnesota Supercomputing Institute (MSI) Itasca cluster up to 1024 processors and on Texas Advanced Computing Center (TACC) Stampede2 Knights Landing cluster upto 8192 processors respectively. Both plots show time taken to generate Arnoldi vectors and Hessenberg matrix for different number of processors. Strong scaling shown in Fig. 1a utilized 101 snapshots of size 64 million each and in Fig. 1b used 201 snapshots of size 240 million each. The snapshot matrix was filled with random numbers as the operation count and scaling properties of the algorithm is independent of the content of the snapshot matrix. Fig. 1a and 1b show good scaling properties of the algorithm on both clusters. Communication avoiding Arnoldi (CA-Arnoldi) of Demmel et al. (2012) which involves delayed orthogonalization can be used in place of standard MGS in algorithm 5. CA-Arnoldi sends lesser number of messages than a standard implementation of Arnoldi. This can also be made use of in the FOADMD framework.

The coefficients  $[c]$  of first snapshot  $\psi_1$  in the basis formed by DMD eigenmodes can be obtained by solving the following matrix problem of size  $(N-1) \times (N-1)$ .

$$\begin{aligned} [\varphi][c] &= \psi_1, \\ [z][c] &= \|\psi_1\|_2 e_1. \end{aligned} \quad (97)$$

If rank truncated FOADMD is used, then the coefficients  $[c]$  of the first snapshot in eigenvector basis can be obtained

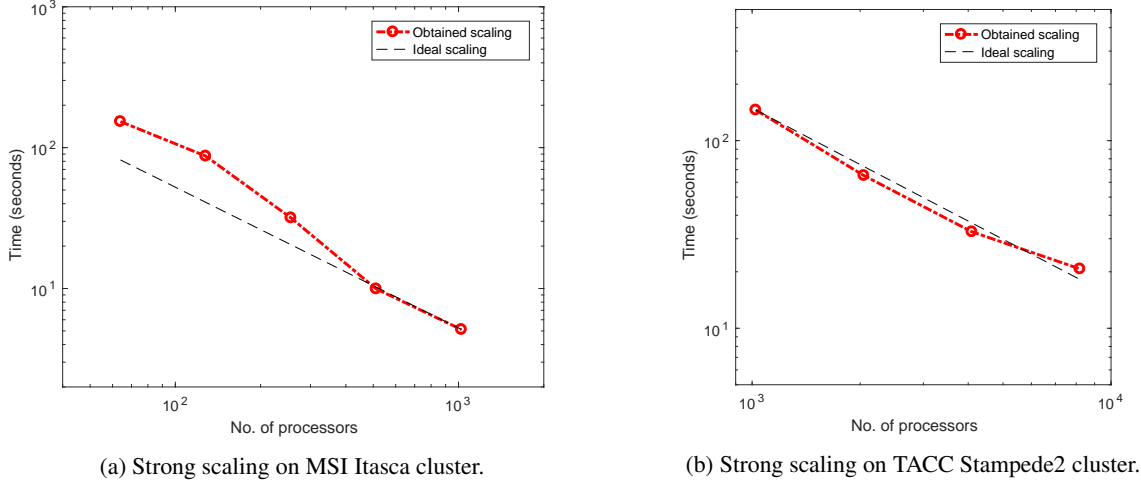


Fig. 1: Strong scaling of modified FOA (Algorithm. 5).

by solving

$$\begin{aligned} [V_1^{N-1} U_r][z][c] &= \psi_1, \\ [z][c] &= \|\psi_1\|_2 U^H e_1. \end{aligned} \quad (98)$$

FOADMD has the streaming property. From algorithm 5, it can be seen that FOADMD only requires the current snapshot  $\psi_j$  to proceed in the Arnoldi iteration. As new snapshots become available, they can be fed into the algorithm to append new orthonormal vectors to the current existing basis vectors and to append new columns to the current upper Hessenberg matrix. Suppose, we have used already  $q$  number of snapshots vectors, the FOADMD implementation to update the upper Hessenberg matrix  $H$ , the set of Arnoldi vectors  $V$  and the  $\beta$  matrix with additional  $p$  number of snapshots stored in  $X$  is given in algorithm 7.

#### 4. Numerical experiments

We illustrate application of FOADMD (algorithm 6) on four problems, i) a synthetic dataset generated from assumed DMD modes and eigenvalues, ii) snapshots that represent vorticity field in a fluid flow over a circular cylinder, iii) snapshots from a linearized channel flow simulation and iv) snapshots from turbulent flow simulation of jets in cross flow.

##### 4.1. Synthetic dataset

A set of snapshots were generated by assuming the DMD modes and eigenvalues. Then algorithm 4 is used to obtain the DMD modes and eigenvalues. Let  $y \in (-10, 10)$  and  $t \in (0, 3\pi)$ . The  $y$ -domain and  $t$ -domain is discretized into finite number of points  $N_y$  and  $N_t$  respectively. The spacing in the  $y$  and  $t$  domains are  $\Delta y = \frac{20}{N_y-1}$  and  $\Delta t = \frac{3\pi}{N_t-1}$ . The  $y$  co-ordinate of  $i^{th}$  point is  $y_i = (i-1)\Delta y$  and  $t$  co-ordinate of  $k^{th}$  point is  $(k-1)\Delta t$ . The  $i^{th}$  component of snapshot

```

1:  $(H, V, AV, \beta, q) = \text{streamingFOADMD } (X, p, H, V, AV, \beta, q)$ 
2: Expand  $H$  to  $p + q \times p + q - 1$  matrix,  $V$  to  $M \times p + q$  matrix,
    $\beta$  to  $p + q \times p + q$  matrix,  $AV$  to  $M \times p + q - 1$  matrix
3:  $jb := q$ 
4: if  $q == 0$  then
5:    $\beta_{1,1} = \|X(:,1)\|_2$ 
6:    $v_1 := \frac{X(:,1)}{\|X(:,1)\|_2}$ 
7:    $jb := 1$ 
8: end if
9: for  $j = jb$  to  $p + q - 1$  do
10:   $AV(:,j) = \frac{1}{\beta_{j,j}} \left( X(:,j+1) - \sum_{k=1}^{j-1} \beta_{k,j} AV(:,k) \right)$ 
11:   $w = AV(:,j)$ 
12:  for  $i = 1$  to  $j$  do
13:     $H_{i,j} = (w, V(:,i))$ 
14:     $w = w - H_{i,j} V(:,i)$ 
15:  end for
16:   $H_{j+1,j} = \|w\|_2; V(:,j+1) = \frac{w}{H_{j+1,j}}$ 
17:   $\beta_{1,j+1} = H(1, 1:j) \beta(1:j, j)$ 
18:  for  $i = 2$  to  $j + 1$  do
19:     $\beta_{i,j+1} = H(i, i-1:j) \beta(i-1:j, j)$ 
20:  end for
21: end for
22:  $q = q + p$ 

```

**Algorithm 7:** Streaming FOADMD implementation.

vector  $x^k$  for  $k = 1, \dots, N_t$  is generated by

$$(x^k)_i = \sum_{j=1}^2 e^{\psi_j(k-1)\Delta t} v_j(y_i); \quad i = 1, \dots, N_y, \quad (99)$$

$$\psi_1 = 2.3i, \quad \psi_2 = 1i,$$

$$v_1(y_i) = 20 - 0.2y_i^2, \quad v_2(y_i) = y_i.$$

$N_t$  and  $N_x$  were chosen to be 10 and 20 respectively. Fig. 2a shows the generated synthetic dataset. The obtained DMD eigenvalues are plotted in fig. 2b. In this case, only 2 linearly independent snapshots are present in the data set. If  $h_{j+1,j}$  at the  $j^{th}$  step of Arnoldi is smaller than a specified tolerance (chosen to be  $10^{-8}$ ) the data set is declared to be linearly dependent and the Arnoldi process is stopped. As mentioned in section 3.4, the obtain DMD eigenvectors and DMD eigenvalues are also the exact eigenvalues and eigenvectors of the linear mapping  $A$  that connects the snapshot vectors. The numerically obtained  $\psi_j$ 's shown in fig. 2b is exactly  $2.3i$  and  $1i$  which are the exponents chosen to generate the dataset. The DMD eigenmodes are plotted in figure 3a and 3b. Within a scaling factor, the eigenmodes are exactly  $v_1$  and  $v_2$  chosen in equation 99. Also, these DMD modes and eigenvalues match (not shown) with those obtained from the standard SVD-based DMD (algorithm 1).

#### 4.2. Linearized channel flow simulation at $Re=10000$

The dataset used to perform DMD analysis of linearized channel flow simulation was obtained from Jovanović et al. (2014). For a description of the numerical method and mesh resolution refer Jovanović et al. (2014). From the same

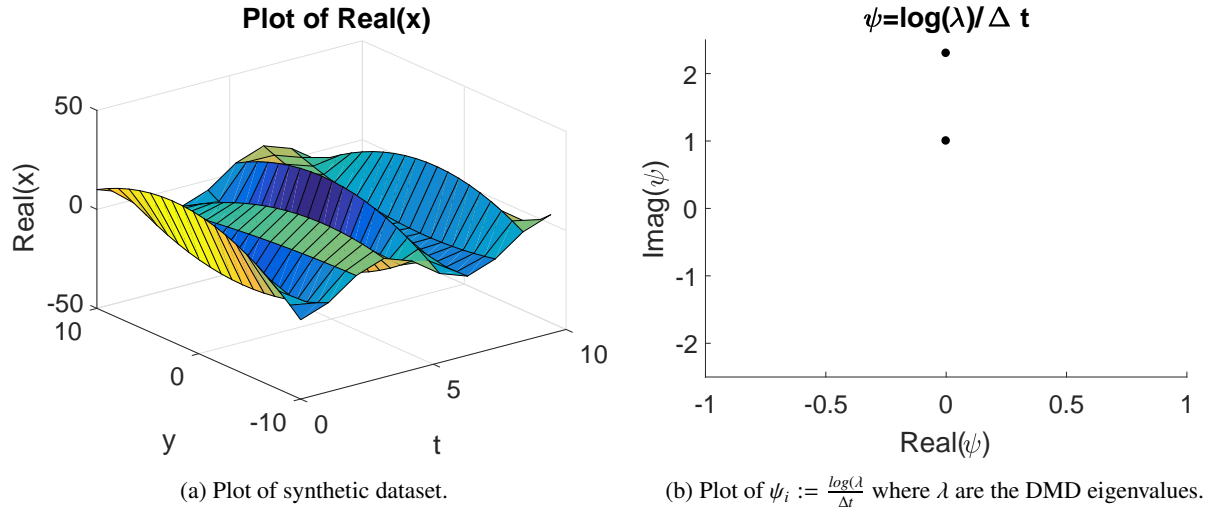


Fig. 2: Synthetic dataset test case.

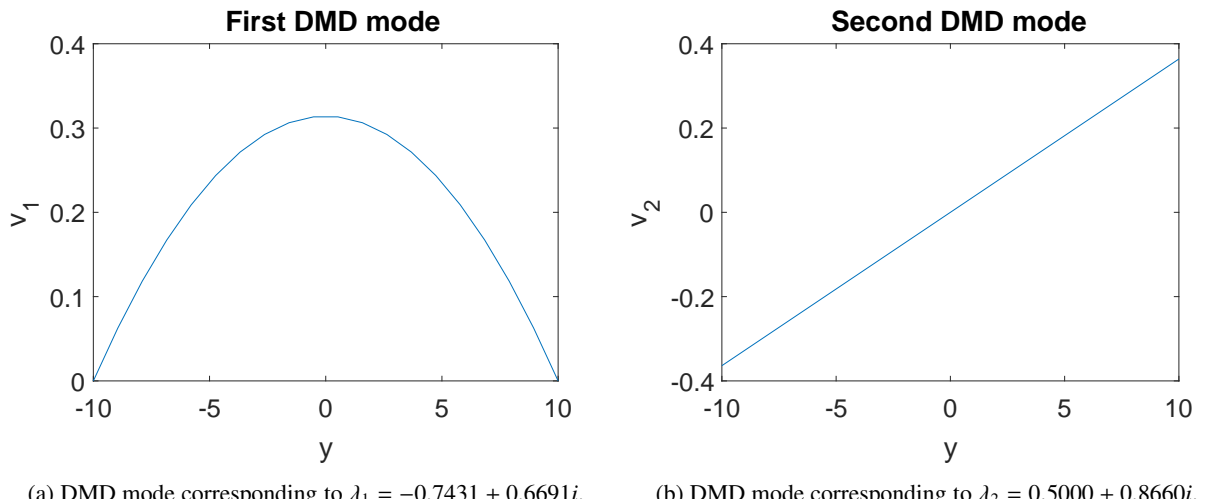
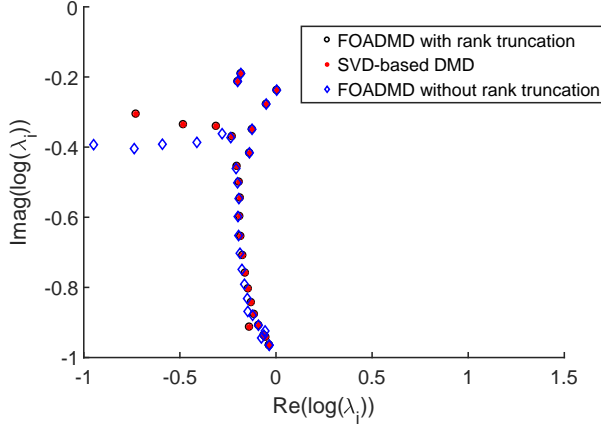


Fig. 3: Synthetic dataset test case.



(a) Comparison of DMD eigenvalues for linearized channel flow simulation snapshots.

	FOADMD	SVD
Without rank truncation	1.4300e+01	6.9241e+00
With rank truncation	4.2750e-04	1.9869e-03

Table 1: Error  $\|P_A - \hat{P}_A\|_2$  in computed projection of  $A$  for both FOADMD and SVD with and without rank truncation for linearized channel flow case.  $P_A$  is the exact projection and  $\hat{P}_A$  is the computed projection.

set of snapshots as used in Jovanović et al. (2014) we compute the DMD eigenvectors and eigenvalues and compare to the SVD based method. The size of each snapshot is 150 and a total of 100 snapshots are used. DMD eigenvalues obtained using FOADMD with and without rank truncation is compared to SVD-based method in figure 4a. The DMD eigenvectors and eigenvalues are ordered based on the values of coefficients obtained by projection of the first snapshot onto the DMD eigenmodes using equation 97.

This dataset is extremely ill-conditioned. The condition number of snapshots evaluated using SVD is  $\approx 10^{17}$ . Even though, 100 snapshots are present, the numerical rank of the dataset is 26. We define numerical rank as the number of singular values of snapshot matrix that are larger than  $N * \text{eps}(\|A\|_2)$ , where  $\text{eps}(x)$  is the distance between  $|x|$  and the next larger double precision floating point number. Also, the linear mapping  $A$  is available. So, we can compute the error involved in projection of  $A$ , DMD eigenvectors and eigenvalues and assess quality of proposed error indicators when the snapshots become extremely ill-conditioned.

Table 1 shows the error in computed projection of  $A$ . The exact projection  $P_A$  is calculated as  $f\ell(Q^H A Q)$ . Since, matrix-matrix multiplication with orthogonal matrix is backward-stable (Higham, 2002), error in evaluation of  $P_A$  will be very small. Finite precision error analysis of SVD-based DMD and FOADMD without rank truncation showed that the error in computed projection is  $O(\kappa_2(X_1^N)\epsilon_m)$ . This is consistent with the numerical results shown in table 1. The increase in accuracy of computed projection with rank truncated versions of SVD and FOADMD seen in table 1 is explained in section 3.2.

Next, we consider the accuracy of computed DMD eigenvectors using FOADMD with and without rank truncation.

Eigenvalue	Error <sub>a</sub>	Error <sub>p</sub>
9.76e-01+(-2.36e-01)i	2.33e-14	4.21e-15
9.14e-01+(-2.60e-01)i	6.26e-11	1.25e-11
8.30e-01+(-3.02e-01)i	3.40e-08	7.43e-09
8.18e-01+(-1.57e-01)i	9.88e-07	1.84e-07
5.62e-01+(-7.19e-01)i	8.80e-06	1.92e-06
5.56e-01+(-7.56e-01)i	5.75e-06	1.22e-06
5.50e-01+(-7.93e-01)i	4.23e-06	8.72e-07
7.97e-01+(-3.52e-01)i	2.30e-06	5.26e-07

Table 2: Comparison of actual error  $\|AV_1^{N-1}z - \lambda V_1^{N-1}z\|_2$  with the predicted error without rank truncation.

Eigenvalue	Error <sub>a</sub>	Error <sub>p</sub>
9.76e-01+(-2.36e-01)i	3.40e-13	3.40e-13
9.14e-01+(-2.60e-01)i	6.00e-10	6.00e-10
8.30e-01+(-3.02e-01)i	1.53e-07	1.53e-07
8.18e-01+(-1.57e-01)i	6.32e-06	6.32e-06
5.62e-01+(-7.20e-01)i	1.30e-05	1.30e-05
5.57e-01+(-7.56e-01)i	5.66e-06	5.66e-06
5.50e-01+(-7.93e-01)i	3.02e-04	3.02e-04
7.97e-01+(-3.52e-01)i	7.57e-06	7.58e-06

Table 3: Comparison of actual error  $\|AV_1^{N-1}U_rz - \lambda V_1^{N-1}U_rz\|_2$  with the predicted error with rank truncation.

tion. Table 2 and 3 shows the comparison of actual error (Error<sub>a</sub>) in eigenvalue-eigenvector pair to the prediction using the error indicator (Error<sub>p</sub>) with and without rank truncation respectively for the 8 DMD modes with least error. The actual error and predicted error is defined as  $\|AV_1^{N-1}z - \lambda V_1^{N-1}z\|_2$  and  $|h_{N,N-1}e_{N-1}^H z|$  respectively for the case without rank truncation and for the case with rank truncation, they are defined as  $\|AV_1^{N-1}U_rz - \lambda V_1^{N-1}U_rz\|_2$  and  $\|V_1^{N-1}(I - U_r U_r^H) H_{N-1} U_r z + h_{N,N-1} v_N e_{N-1}^H U_r z\|_2$  respectively where  $\lambda$  and  $z$  are the eigenvalue and eigenvector pair of the projected problem. As, we can see from table 2 and 3, the error in dominant eigenvalues and corresponding eigenvectors are of the same order of magnitude. However, the predicted error is more close to the actual error for the case with rank truncation than without rank truncation. This is because of the smaller backward error for the Arnoldi relation (equation 85) for the case with rank truncation.

#### 4.3. Flow over cylinder at $Re=100$

We consider the flow over a circular cylinder at Reynolds number ( $Re := VD/\nu$ ) of 100 ( $V$ ,  $D$  and  $\nu$  denote freestream velocity, diameter of cylinder and kinematic viscosity of fluid respectively). The data set for this case is obtained from Kutz et al. (2016). For details on the numerical method used to generate the cylinder snapshots refer Kutz et al. (2016). A total of 151 snapshots of vorticity field separated by time interval  $\Delta t = 0.02$  were used. Fig. 5a shows a snapshot of the vorticity field. The cylinder is placed at (0,0) and the diameter of the cylinder is 1. The flow is from left to right. It is known that as we increase  $Re$ , for  $Re > 47$  vortices are shed from the cylinder at a particular frequency dependent on  $Re$ . These vortices can be clearly seen from fig. 5a. At  $Re = 100$ , the Strouhal number  $St = fD/V$  is 0.16. We can capture this frequency by performing DMD of the snapshots of vorticity field.

Fig. 5b compares DMD eigenvalues associated with 21 dominant eigenmodes from the proposed FOADMD method (without truncation) and SVD-based technique. The DMD eigenmodes from FOADMD are ranked based on the magnitude of  $c_j$  when the first snapshot  $x_1$  is represented in the basis of DMD eigenmodes (equation 97). Also, only few of the computed DMD eigenmodes have sufficiently large values of  $c_j$  (not shown). These DMD eigenmodes give an appropriate basis to represent the dataset. In SVD-based DMD technique, only the first 21 singular vectors are used to evaluate the DMD eigenvalues and eigenmodes. The eigenvalues from both techniques is compared in fig. 5b and they show good agreement.

Figs. 6a and 6b show the first 2 dominant DMD eigenmodes. DMD eigenmode in 6a has DMD eigenvalue of 1 and represents the mean vorticity field. The second dominant DMD eigenmode shown in figure 6b corresponds to the

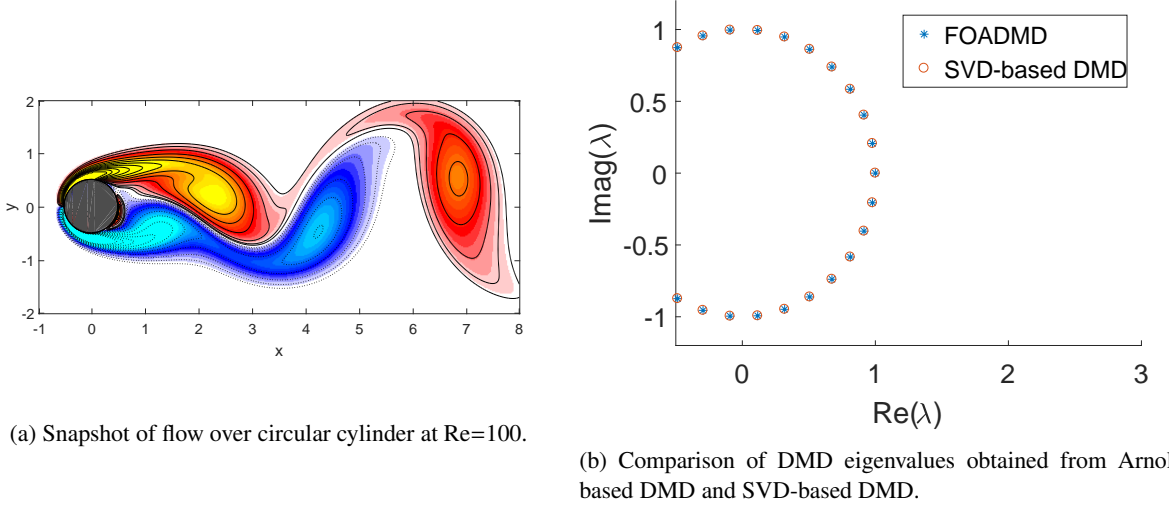


Fig. 5: Cylinder test case.

$\frac{\log(\lambda)}{2\pi\Delta t}$	$Error_{DMD}$
$-0.0000+(0.0000)i$	$2.65e-08$
$0.0000+(1.6540)i$	$8.17e-08$
$0.0000+(-1.6540)i$	$8.17e-08$
$-0.0000+(3.3079)i$	$2.25e-07$
$-0.0000+(-3.3079)i$	$2.25e-07$

Table 4: Predicted error in DMD eigenvector and eigenvalues for the 5 most dominant eigenvalues.

vortex shedding frequency. The frequency of oscillation of DMD mode is given by  $imag(\log(\lambda)/(2\pi\Delta t))$  where  $\lambda$  is corresponding DMD eigenvalue. Fig. 6b corresponds to DMD eigenvalue,  $\lambda = 0.9875 - 0.2063i$  whose associated frequency is 0.1654, which is exactly the  $St$  at  $Re = 100$ .

The condition number of the snapshots for flow over cylinder at  $Re=100$  is  $\approx 10^7$ . Also, the snapshots matrix is full rank (measured using numerical rank). So, rank truncation is not required for this case. Table 4 shows the quality of the five most dominant DMD eigenvectors and eigenvalues. Since, the condition number of the snapshots is very small when compared with  $\frac{1}{\epsilon_m}$ , the computed error indicator  $|h_{N,N-1}e_{N-1}^H z|$  should be close to the actual error  $\|AV_1^{N-1}z - \lambda V_1^{N-1}z\|_2$ .

#### 4.4. Jets in cross flow

Next, we consider a large dataset obtained from Direct Numerical Simulation (DNS) of turbulent jets in cross flow. DMD on this dataset has been previously performed by Iyer and Mahesh (2016) using the algorithm of Rowley et al. (2009). Here, we use FOADMD to obtain the DMD modes and eigenvalues and compare to previously obtained results. For more information on the problem, simulation, timestep and grid, the reader is referred to Iyer and Mahesh (2016). Here, we consider jet velocity to cross-flow velocity ratios (R) of 2 and 4. The size of each snapshot is 240 million. A total of 80 snapshots were used for R=4, and 250 snapshots were used for R=2 case.

The parallel implementation discussed in section 3.4 was used. The data was split row-wise among different

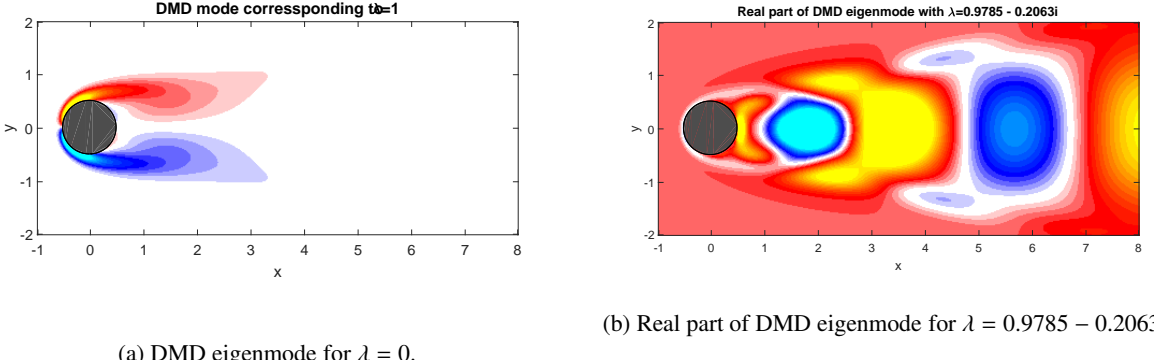


Fig. 6: Cylinder test case.

R	Previous result Iyer and Mahesh (2016)	FOADMD	Error <sub>DMD</sub>
2	0.6255	0.6263	0.0194
2	1.2077	1.2071	0.0323
4	0.3804	0.3804	0.0545
4	0.7624	0.7621	0.0518

Table 5: Comparison of Strouhal number associated with shear layer modes obtained from FOADMD and result of Iyer and Mahesh (2016) for different jet velocity to cross flow velocity ratios (R) and the predicted error associated with DMD eigenvalues and eigenvectors.

processors. A total of 512 processors were used to process the data. The condition number of snapshot matrix is  $\approx 10^2$  which is very small when compared with machine epsilon for double precision datatype. So, FOADMD without rank truncation is used to compute the DMD eigenvalues and eigenvectors. Also, in Iyer and Mahesh (2016), DMD eigenvalues and eigenvectors were obtained through the projected companion matrix (equation 9). The normal equations for the last column of the companion matrix was solved using rank truncated SVD. Table 5 shows the good agreement of the Strouhal number (non-dimensionalized with peak jet velocity and diameter of orifice) associated with shear layer modes obtained from FOADMD with Iyer and Mahesh (2016). Also, the computed error indicator  $|h_{N,N-1}e_{N-1}^H z|$  presented in table 5 shows the better quality of eigenvectors for R=2 case than R=4. This is because of a larger set of snapshots used for R=2 than R=4. Fig. 7 shows the Q-criterion of shear layer modes at R=2 and R=4 and they agree with those obtained by Iyer and Mahesh (2016).

## 5. Conclusion

In this paper, we develop a modified version of the standard FOA method, which forms the kernel of the proposed FOADMD algorithm (algorithm 6). From finite precision error analysis of the FOADMD, the accuracy of computed projection of the linear mapping  $A$  is shown to be  $O(\kappa_2(X_1^{N-1})\epsilon_m)$  which is same as that for SVD based methods. For snapshots with extremely large condition numbers of  $O(\frac{1}{\epsilon_m})$ , rank truncated FOADMD is proposed. The increase in accuracy of computed projection onto a subspace of Krylov subspace in rank truncated FOADMD method is explained using finite precision error analysis. Error indicators for the computed DMD eigenvectors and eigenvalues are derived for FOADMD and the rank truncated version. These error indicators can be used to devise stopping criterion for

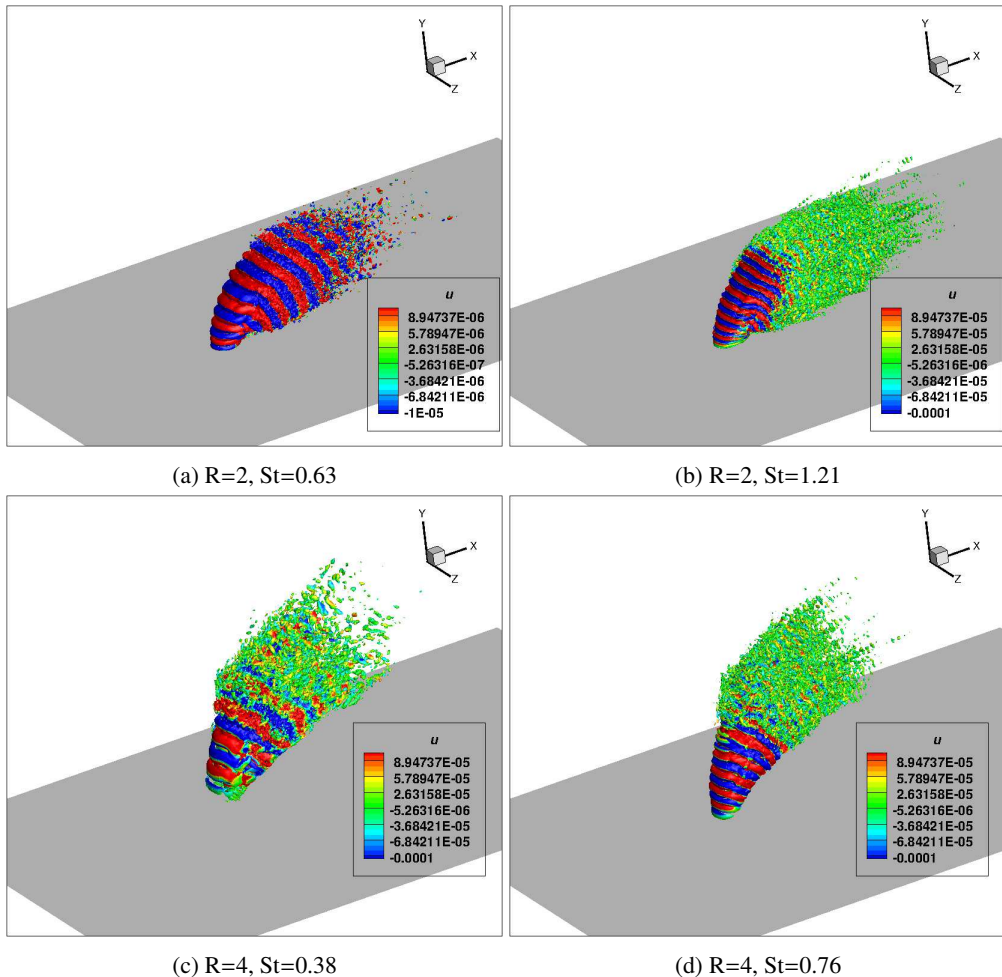


Fig. 7: Real part of DMD eigenmode associated with shear layer.

DMD. Exact reconstruction property, operation count, streaming and parallel implementation aspects of the proposed method are discussed. The method is easily parallelizable, thus making it attractive to process large datasets stored on parallel computers. Scaling of the algorithm is shown upto 8192 processors. The proposed algorithm is tested on four cases of increasing levels of dimensionality and condition number of snapshot matrix. The proposed error indicators are validated and bounds of accuracy of computed projection is assessed using linearized channel flow simulation snapshots at  $Re = 10000$ . The DMD eigenvectors and eigenvalues are extracted from cylinder simulation snapshots at  $Re = 100$  using FOADMD and compared with those obtained by SVD-based methods. The capability of the method to perform DMD on very large scale datasets is shown by performing DMD of snapshots obtained from DNS of turbulent jet in cross flow at two different jet velocity to cross flow velocity ratios.

## Acknowledgement

The authors would like to acknowledge support by AFOSR under grant FA9550-15-1-0261. The scaling study was made possible through computing resources provided by Minnesota Supercomputing Institute (MSI) and Texas Advanced Computing Center (TACC). The authors would like to thank Dr. Prahладh Iyer for providing the jets in cross flow dataset.

## Appendix

### Appendix A. Estimate of $E_5 := \hat{V}_1^{N-1} - X_1^{N-1}\hat{a}_1^{N-1}$ for Arnoldi-based DMD variant-1.

The first column of  $E_5$  is  $E_5(:, 1) = \hat{v}_1 - \psi_1 \hat{a}_{1,1}$ , where  $\hat{a}_{1,1} := fl(1/fl(\|\psi_1\|_2))$  and  $\hat{v}_1 = fl(\psi_1/\|\psi_1\|_2)$ . Using finite-precision arithmetic model (Higham, 2002),

$$E_5(:, 1) = \frac{\psi_1}{\|\psi_1\|_2} 2\theta_{2M+1}, \quad (\text{A.1})$$

where  $|\theta_{2M+1}| \leq \gamma_{2M+1}$ . The 2<sup>nd</sup> to  $N - 1$  columns of  $E_5$  can be estimated as follows. From finite precision  $(j - 1)^{th}$  step of Algorithm. 5, we have

$$\hat{h}_{j,j-1}\hat{v}_j = fl(w_{j-1}) - \sum_{i=1}^{j-1} \hat{h}_{i,j-1}\hat{v}_i - E_3(:, j-1); j = 2, \dots, N-1. \quad (\text{A.2})$$

Adding and subtract  $w_{j-1}$  in right hand side of above equation and replacing  $v_i$ ,

$$\hat{h}_{j,j-1}\hat{v}_j = w_{j-1} - \sum_{i=1}^{j-1} \hat{h}_{i,j-1} \left( \sum_{k=1}^i \hat{a}_{k,i} \psi_k + E_5(:, i) \right) - E_3(:, j-1) + E_4(:, j-1); j = 2, \dots, N-1. \quad (\text{A.3})$$

Let  $E^{fl_a}(:, j) := \hat{h}_{j,j-1} \sum_{i=1}^j (\tilde{a}_{i,j} - \hat{a}_{i,j}) x_i$ ;  $j = 2, \dots, N - 1$  be the error due to finite precision computation of  $a_{:,j}$ , where  $\tilde{a}_{1:j,j}$  is the exact  $j^{th}$  column computed using  $\hat{a}_{1:j-1,1:j-1}$  and  $\hat{h}_{1:j,1:j-1}$  using equation 26. Then,

$$\begin{aligned} \hat{h}_{j,j-1}\hat{v}_j &= \hat{h}_{j,j-1} \sum_{i=1}^j \hat{a}_{i,j} x_i + E^{fl_a}(:, j) - \sum_{i=1}^{j-1} \hat{h}_{i,j-1} E_5(:, i) + E_4(:, j-1) - E_3(:, j-1); j = 2, \dots, N-1 \\ \hat{h}_{j,j-1} E_5(:, j) &= - \sum_{i=1}^{j-1} \hat{h}_{i,j-1} E_5(:, i) + E^{fl_a}(:, j) + E_4(:, j-1) - E_3(:, j-1); j = 2, \dots, N-1 \end{aligned} \quad (\text{A.4})$$

Rearranging, using the estimate of first column of  $E_5(:, 1)$ , the definition of  $\hat{R}_N$  and a bound for  $\hat{R}_N(1 : N - 1, 1 : N - 1)^{-1}$  using perturbation of singular values result (Higham, 2002), we get

$$\begin{aligned} E_5 \hat{R}_N(1 : N - 1, 1 : N - 1) &= [E_5(:, 1), E^{fl_a}(:, 2 : N - 1) + E_4(:, 1 : N - 2) - E_3(:, 1 : N - 2)], \\ \|E_5\|_F &\leq C(2\gamma_{2M+1} + \|E^{fl_a}(:, 2 : N - 1)\|_F + \|E_4(:, 1 : N - 2)\|_F + \|E_3(:, 1 : N - 2)\|_F), \\ C &:= \frac{1}{\sigma_{N-1}([\hat{v}_1, fl(W_1^{N-2})]) - \sqrt{N}c_2\epsilon_m\sigma_1([\hat{v}_1, fl(W_1^{N-2})])}, \end{aligned} \quad (\text{A.5})$$

where  $\sigma_1([\hat{v}_1, fl(W_1^{N-2})])$  and  $\sigma_{N-1}([\hat{v}_1, fl(W_1^{N-2})])$  are the first and  $(N-1)^{th}$  singular value of the matrix  $[\hat{v}_1, fl(W_1^{N-2})]$ .

Using the finite precision version of equation 26, we obtain the size of  $\|E^{fl}(:, 2 : N - 1)\|_F$

$$\|E^{fl}(:, 2 : N - 1)\|_F \leq \gamma_N \|X_1^{N-1}\|_2 \left( \|\hat{\alpha}_{N-1}\|_2 \|\hat{H}_{N-1}\|_F + \|\hat{\alpha}_{N-1}\|_F \right) \quad (\text{A.6})$$

Using equation 37, 40 and A.6 in A.5, we get the equation 43 estimate for  $\|E_5\|_F$ .

## References

K. Taira, S. L. Brunton, S. Dawson, C. W. Rowley, T. Colonius, B. J. McKeon, O. T. Schmidt, S. Gordeyev, V. Theofanis, L. S. Ukeiley, Modal analysis of fluid flows: An overview, arXiv preprint arXiv:1702.01453 (2017).

C. W. Rowley, S. T. Dawson, Model reduction for flow analysis and control, *Annual Review of Fluid Mechanics* 49 (2017) 387–417.

C. W. Rowley, I. Mezić, S. Bagheri, P. Schlatter, D. S. Henningson, Spectral analysis of nonlinear flows, *Journal of fluid mechanics* 641 (2009) 115–127.

I. Mezić, Analysis of fluid flows via spectral properties of the koopman operator, *Annual Review of Fluid Mechanics* 45 (2013) 357–378.

P. Schmid, J. Sesterhenn, Dynamic mode decomposition of numerical and experimental data, in: APS Meeting Abstracts, 2008.

P. J. Schmid, Dynamic mode decomposition of numerical and experimental data, *Journal of fluid mechanics* 656 (2010) 5–28.

J. H. Tu, C. W. Rowley, D. M. Luchtenburg, S. L. Brunton, J. N. Kutz, On dynamic mode decomposition: theory and applications, arXiv preprint arXiv:1312.0041 (2013).

M. S. Hemati, M. O. Williams, C. W. Rowley, Dynamic mode decomposition for large and streaming datasets, *Physics of Fluids* 26 (2014) 111701.

M. O. Williams, I. G. Kevrekidis, C. W. Rowley, A data–driven approximation of the koopman operator: Extending dynamic mode decomposition, *Journal of Nonlinear Science* 25 (2015) 1307–1346.

M. O. Williams, C. W. Rowley, I. G. Kevrekidis, A kernel-based approach to data-driven koopman spectral analysis, arXiv preprint arXiv:1411.2260 (2014).

M. R. Jovanović, P. J. Schmid, J. W. Nichols, Sparsity-promoting dynamic mode decomposition, *Physics of Fluids* 26 (2014) 024103.

T. Sayadi, P. J. Schmid, Parallel data-driven decomposition algorithm for large-scale datasets: with application to transitional boundary layers, *Theoretical and Computational Fluid Dynamics* 30 (2016) 415–428.

J. Demmel, L. Grigori, M. Hoemmen, J. Langou, Communication-optimal parallel and sequential qr and lu factorizations, *SIAM Journal on Scientific Computing* 34 (2012) A206–A239.

D. Duke, J. Soria, D. Honnery, An error analysis of the dynamic mode decomposition, *Experiments in Fluids* 52 (2012) 529–542.

H. Zhang, S. Dawson, C. W. Rowley, E. A. Deem, L. N. Cattafesta, Evaluating the accuracy of the dynamic mode decomposition, arXiv preprint arXiv:1710.00745 (2017).

L. N. Trefethen, D. Bau III, *Numerical linear algebra*, volume 50, Siam, 1997.

Y. Saad, Variations on arnoldi's method for computing eigenelements of large unsymmetric matrices, *Linear algebra and its applications* 34 (1980) 269–295.

Y. Saad, *Numerical Methods for Large Eigenvalue Problems: Revised Edition*, SIAM, 2011.

N. J. Higham, *Accuracy and stability of numerical algorithms*, volume 80, Siam, 2002.

Å. Björck, C. C. Paige, Loss and recapture of orthogonality in the modified gram–schmidt algorithm, *SIAM journal on matrix analysis and applications* 13 (1992) 176–190.

L. Giraud, J. Langou, M. Rozložník, J. van den Eshof, Rounding error analysis of the classical gram–schmidt orthogonalization process, *Numerische Mathematik* 101 (2005) 87–100.

J. Drkošová, A. Greenbaum, M. Rozložník, Z. Strakoš, Numerical stability of gmres, *BIT Numerical Mathematics* 35 (1995) 309–330.

H. F. Walker, Implementation of the gmres method using householder transformations, *SIAM Journal on Scientific and Statistical Computing* 9 (1988) 152–163.

G. H. Golub, C. F. Van Loan, *Matrix computations*, volume 3, JHU Press, 2012.

J. N. Kutz, S. L. Brunton, B. W. Brunton, J. L. Proctor, Dynamic mode decomposition: Data-driven modeling of complex systems, 2016.

P. S. Iyer, K. Mahesh, A numerical study of shear layer characteristics of low-speed transverse jets, *Journal of Fluid Mechanics* 790 (2016) 275–307.